

University of Nebraska - Lincoln

DigitalCommons@University of Nebraska - Lincoln

---

Mechanical (and Materials) Engineering --  
Dissertations, Theses, and Student Research

Mechanical & Materials Engineering, Department  
of

---


8-2018

# Design of Parallel Robot for Dental Articulation and Its Optimization

Abulimiti Delimulati

University of Nebraska-Lincoln, [dilmurat@huskers.unl.edu](mailto:dilmurat@huskers.unl.edu)

Follow this and additional works at: <http://digitalcommons.unl.edu/mechengdiss>

 Part of the [Applied Mechanics Commons](#), [Biomechanical Engineering Commons](#), [Dental Materials Commons](#), and the [Prosthodontics and Prosthodontology Commons](#)

---

Delimulati, Abulimiti, "Design of Parallel Robot for Dental Articulation and Its Optimization" (2018). *Mechanical (and Materials) Engineering -- Dissertations, Theses, and Student Research*. 140.

<http://digitalcommons.unl.edu/mechengdiss/140>

This Article is brought to you for free and open access by the Mechanical & Materials Engineering, Department of at DigitalCommons@University of Nebraska - Lincoln. It has been accepted for inclusion in Mechanical (and Materials) Engineering -- Dissertations, Theses, and Student Research by an authorized administrator of DigitalCommons@University of Nebraska - Lincoln.

**DESIGN OF PARALLEL ROBOT FOR DENTAL ARTICULATION AND ITS  
OPTIMIZATION**

by

Abulimiti Delimulati

A THESIS

Presented to the Faculty of

The Graduate College at the University of Nebraska

In Partial Fulfilment of Requirements

For the Degree of Master of Science

Major: Mechanical Engineering and Applied Mechanics

Under the Supervision of Professor Carl A. Nelson

Lincoln, Nebraska

August 2018

# DESIGN OF PARALLEL ROBOT FOR DENTAL ARTICULATION AND ITS OPTIMIZATION

Abulimiti Delimulati M.S.

University of Nebraska, 2018

**Advisor:** Carl A. Nelson

A dental articulator is a mechanical device used to simulate the relative position and motion between the upper and lower jaw when constructing and testing dental prostheses. Typically, it can be adjusted to approximate patient-specific jaw kinematics in order to analogue the static relationship and specific motions of a patient's mandible to maxilla. However, the use of dental articulators is essentially a trial-and-error method in order to fine-tune fit and function of a dental prosthesis. Some of the most advanced current dental articulators can reproduce the position and the motion passively; furthermore, dentists need special training for measuring patients' maxillofacial dimensions. Moreover, masticatory robots developed for training purposes cannot mimic individual patients' jaw motions.

The thesis presents the design and optimization of parallel robot for dental articulation. In this design we propose a robotic articulator suitable for reproducing tracked movements of an individual patient's jaw. Based on an asymmetric-leg parallel structure, dimensional synthesis is performed to optimize performance over the range of motion typical of the human jaw. The resulting robotic device is expected to improve workflow in the restoration of dental implants.

**Keywords:** dental, articulator, jaw, motion, position, robotics, mandible, maxilla, condyle, parallel robot, dental implant.

**Citation:** Delimulati, A. 2018, 'Design of Parallel Robot for Dental Articulation and Its Optimization', M.Sc. Thesis, University of Nebraska-Lincoln, Lincoln, NE, USA

*“The problem of articulation could only be solved when dentistry succeeded to record and reproduce jaw movements of individual patients.”*

--A. Gysi 1907

## **Acknowledgements:**

*First of all, I would like to thank my advisor, Dr. Carl A. Nelson, for his support and guidance throughout this project. I would like to thank my fellow colleagues, especially Nathan Borcyk for his support and contributions. Without them, this work would not have been possible.*

*I would like to thank my parents for their endless love and support. They are the foundation of who I am today, and I am forever grateful for everything they have done.*

*Finally, I would like to thank my incredible wife Ehtibar and lovely daughters Dilziba, Dilnawa and Dilara. Their unending love, patience, and encouragement have allowed me to pursue my dreams.*





## Table of Contents

List of Figures .....	vii
List of Tables.....	viii
List of terms and Symbols .....	viii
Terms.....	viii
2. Symbols.....	xiv
Chapter 1: Introduction.....	1
Historical background and current devices in practice .....	1
1.2 Developments in dental engineering.....	3
1.3 Virtual Articulator .....	5
1.4 Summary and Drawbacks.....	6
Chapter 2: Notion of the Idea.....	8
Chapter 3: Approach.....	11
3.1. Workspace and Movements of the Human Mandible .....	11
3.1.1 Functional Anatomy of Masticatory System .....	11
3.1.2 Border and Functional Movements of Human Mandible.....	12
3.2. 6-RSS Architecture for Dental articulator.....	19
3.3. Inverse Kinematics.....	22
Chapter 4: Design and Optimization.....	26
Chapter 5: Physical Design.....	34
5.1 Mechanical Components .....	34
5.2 Electronic Components .....	36
5.3 The Prototype of the Robot .....	38
5.4 Manufacturing and Prototype Testing.....	40
Chapter 6: Conclusions and Future Work.....	44
6.1 Conclusions .....	44
6.2 Future Work: .....	44
References.....	46
Appendix.....	50
Appendix A .....	50
A-1 Creating 6D hypercube vectors within the workspace.....	50



A-2 Calculating P, Q, S, H, h1, and h2 values corresponding to the vectors we derived for each leg.....	50
A-4 code for finding the vector AC's value and maximum and minimum values of AC for each leg.....	53
A-5 Ultimate values for $l_{1i}$ and $l_{2i}$ .....	55
A-6 Testing Robot .....	57
Appendix B .....	58
B-1 Code for finding the revolute range of Servo .....	58
B-2 Code for the opening-closing movement.....	59
Appendix C .....	62
C-1 Ball Socket Cab .....	62
C-2 End Effector.....	63
C-3 First Link of Leg.....	63
C-4 Part A of Base.....	64
C-5 Part B of Base .....	64
C-6 Part 1 of Frame .....	65
C-7 Part 2 of Frame .....	65
C-8 Part 3 of Frame .....	66
C-9 Part 4 of Frame .....	66
C-10 HS - 5065MG Servo .....	67
C-11 Arduino UNO .....	69

## List of Figures

Figure 2. 1 Robotic Dental Articulator Concept.....	9
Figure 3. 1 Movement of Mandible .....	14
Figure 3. 2 Border and Functional Movements in Sagittal Plane.....	15
Figure 3. 3 Border and Functional Movements in Horizontal Plane .....	16
Figure 3. 4 Border and Functional Movements in Frontal Plane.....	17
Figure 3. 5 Envelope or Workspace of the Mandible in 3 Dimensional Space .....	18
Figure 3. 6 6-RSS Architecture for Dental Articulator.....	19
Figure 3. 7 Vector-Loop Closures .....	21
Figure 3. 8 The End Effector of the Robot .....	23
Figure 3. 9 Base Frame .....	23
Figure 4. 1 Workspace Assumption.....	27
Figure 4. 2 the Maximum Range of Motion .....	28
Figure 4. 3 Initial Optimization of First and Second Leg.....	29
Figure 4. 4 Flowchart of the Optimization Process .....	31
Figure 4. 5 CAD Model of Optimized Robot .....	32
Figure 5. 1 Second Link of The Leg ( $l_{2i}$ ) .....	34
Figure 5. 2 CAD Designs of Parts .....	35
Figure 5. 3 3D Printed Mechanical Parts .....	36
Figure 5. 4 Electronic Components .....	37

Figure 5. 5 The Prototype of the Robot .....	38
Figure 5. 6 Comparison of the Robot and Denar Articulator .....	39

### **List of Tables**

Table 4. 1 Design Variables and Parameters .....	26
Table 4. 2 Iterations and $l_{1i}$ and $l_{2i}$ Values (mm).....	32
Table 4. 3 Optimized Legs' Length Parameters .....	33

### **List of terms and Symbols**

#### **Terms**

Alveolar bone – the thickened ridge of bone that contains the tooth sockets (dental alveoli) on bones that hold teeth.

Arcon articulator – an articulator with the equivalent condylar guides fixed to the upper member and the hinge axis to the lower member.

Articular disc – a thin, oval plate of fibrocartilage present in several joints which separates synovial cavities

Articular eminence – a bony eminence on the temporal bone in the skull.

Balanced occlusion – the simultaneous contacting of the upper and lower teeth on the right and left and in the anterior and posterior occlusal areas in centric and eccentric positions within the functional range; used primarily in reference to the mouth, but also

arranged and observed on articulators, developed to prevent tipping or rotating of denture bases in relation to supporting structures.

Bennett angle – the angle formed by the sagittal plane and the path of the advancing condyle during lateral mandibular movements as viewed in horizontal plane.

Bite block – a wedge-shaped implement used in dentistry for dentists working with children and other patients who have difficulty keeping their mouths open wide and steady during a procedure, or during procedures where the patient is sedated.

Rami – plural of ramus that is a small branchlike structure extending from a larger one or dividing into two or more parts, such as a branch of a nerve or artery or one of the rami of the blood vessel or nerve.

Bridge – A bridge is a fixed dental restoration (a fixed dental prosthesis) used to replace one or more missing teeth by joining an artificial tooth definitively to adjacent teeth or dental implants.

Bristol parallel robot – a parallel robot to test dental components and materials.

Capsule ligaments – found on the outer surface of the capsule, simply thickenings of the fibrous capsule itself that take the form of either elongated bands or triangles, the fibers of which radiate from a small area of one articulating bone to a line upon its mating fellow.

Cast – a positive copy or mold of the tissues of the jaws, made in an impression, and over which denture bases or other restorative materials may be fabricated.

Cementum – a layer of bonelike, mineralized tissue covering the dentin of the root and neck of a tooth that anchors the fibers of the periodontal ligament.

Centric relation (CR) – the mandibular jaw position in which the head of the condyle is situated as far posteriorly and superiorly as it possibly can within the mandibular fossa/glenoid fossa.

Collateral ligaments – one of a pair of ligaments occurring on the medial or lateral sides of hinge joints that typically serve a major role in uniting the articulating bones and establish the radius of movement for the joint.

Condylar – is the round prominence at the end of a bone, most often part of a joint - an articulation with another bone.

Degree of freedom (DOF) – the number of parameters of the system that may vary independently.

Dental model – something that represents or simulates denture or teeth; a dental replica.

Gingiva – the part of the oral mucosa covering the tooth-bearing border of the jaw; called also gum.

Global dental arch – the curved composite structure of the natural dentition and the residual ridge, or the remains thereof after the loss of some or all-natural teeth.

Gnathic – pertaining to the jaw or cheeks.

Implant (Endosseous) – a surgical component that interfaces with the bone of the jaw or skull to support a dental prosthesis such as a crown, bridge, denture, facial prosthesis or to act as an orthodontic anchor.

Incisal guidance – the influence on mandibular movements caused by the contacting surfaces of the mandibular and maxillary anterior teeth during eccentric excursions.

Joint capsule – the saclike envelope that encloses the cavity of a synovial joint by attaching to the circumference of the articular end of each involved bone

Mandible – the largest, strongest and lowest bone in the human face

Mandibular fossa – the depression in the temporal bone that articulates with the mandible.

Maxilla – the upper jawbone formed from the fusion of two maxillary bones.

Midpalatal suture – the lines of junction between the palatal bones of the skull at the midline.

Nonarcon articulator – an articulator with the equivalent condylar guides attached to the lower member and the hinge axis to the upper member.

Occlusal relationship – the relationship of the mandibular teeth to the maxillary teeth when they are in a defined contact position.

Orthodontics – a specialty field of dentistry that deals primarily with malpositioned teeth and the jaws: their diagnosis, prevention and correction.

Periodontal ligament – a group of specialized connective tissue fibers that essentially attach a tooth to the surrounding alveolar bone

Prosthodontics – the area of dentistry that focuses on dental prostheses.

Sphenomandibular ligament – a flat, thin band which is attached superiorly to the spina angular surface (spine) of the sphenoid bone, and, becoming broader as it descends, is fixed to the lingual of the mandibular foramen.

Stylomandibular ligament – the thickened posterior portion of the investing cervical fascia, which extends from near the apex of the styloid process of the temporal bone to the angle and posterior border of the angle of the mandible, between the masseter and medial pterygoid.

Synovial articulation – also known as diarthrosis, joins bones with a fibrous joint capsule that is continuous with the periosteum of the joined bones, constitutes the outer boundary of a synovial cavity, and surrounds the bones' articulating surfaces.

Temporal bone – situated at the sides and base of the skull, and lateral to the temporal lobes of the cerebral cortex.

Temporomandibular ligament – consists of two short, narrow fasciculi, one in front of the other, attached, above, to the lateral surface of the zygomatic arch and to the tubercle on its lower border; below, to the lateral surface and posterior border of the neck of the mandible.

The lateral pterygoid muscle – a muscle of mastication with two heads. It lies superiorly to the medial pterygoid. The superior head originates on the infratemporal surface and infratemporal crest of the greater wing of the sphenoid bone and inserts onto the articular disc and fibrous capsule of the temporomandibular joint. The inferior head originates on the lateral surface of the lateral pterygoid and inserts onto the neck of condyloid process of the mandible.

The masseter muscle – The major jaw muscle, which participates in protraction, retraction and side to side movement of the jaw. Its superficial portion originates from the maxillary process of the zygomatic bone, and the anterior two-thirds of the inferior border of the zygomatic arch and inserts into the angle and ramus of the mandible; its deep portion originates from the deep and medial surface of the zygomatic arch and inserts the angle and ramus of the mandible.

The medial pterygoid muscle – a thick, quadrilateral muscle of mastication. The bulk of the muscle arises as a deep head from just above the medial surface of the lateral pterygoid plate. The smaller, superficial head originates from the maxillary tuberosity and the pyramidal process of the palatine bone. Both are inserted by a strong tendinous lamina, into the lower and back part of the medial surface of the ramus and angle of the mandible, as high as the mandible foramen.

The temporalis muscle – one of the muscles of mastication. It is a broad, fan-shaped muscle on each side of the head that fills the temporal fossa, superior to the zygomatic arch so it covers much of the temporal bone. It arises from the temporal fossa and the deep part of temporal fascia. It passes medial to the zygomatic arch and forms a tendon which inserts onto the coronoid process of the mandible, with its insertion extending into the retromolar fossa posterior to the most distal mandibular molar.

TMJ ligaments – Bundles of a tough, fibrous, elastic protein called collagen that act to bind and support the TMJ.

U-shaped bone – also called tongue bone or hyoid bone, a horseshoe-shaped bone situated in the anterior midline of the neck between the chin and the thyroid cartilage.



Workspace – the set of points that can be reached by its end-effector or, in other words, it is the space in which the robot works and can be either a 3D space or a 2D surface.

---

## 2. Symbols

6-RSS: 6-leg revolute/spherical/spherical parallel robot architecture

6-SPS: 6-leg spherical/prismatic/spherical parallel robot architecture

$A_i$ : a point at first joint

$a_i$ : an angle about z-axis at fixed platform

$B_i$ : a point at second joint

$c$ : cosine

$C_i$ : a point at third joint

CR: Centric relation

F: degrees of freedom of the robot

$f_i$ : degree of relative motion permitted by joint  $i$

$f_p$ : the total number of passive degrees of freedom

fzero: a Matlab function

$H_{\max}$ : the maximum protrusion

$j$ : the number of binary joints of the mechanism

$l_{11}$ : the first link of leg

$l_2$ : the second link of leg

$L_{\max}$ : the maximum mouth-opening movement

$n$ : the number of links in the manipulator including the base

O: fixed frame

${}^O\mathbf{A}$ ,  ${}^O\mathbf{B}$ ,  ${}^O\mathbf{C}$ ,  ${}^O\mathbf{D}$ : vector points as referenced to frame O

P: moving frame

$\mathbf{R}$ : rotation matrix

$r_1$ : the distance from center of fixed frame to first joint

$r_2$ : the distance from center of moving frame to third joint

$\mathbf{R}_{x,\phi}$ : rotation matrix about x-axis with pitch angle

$\mathbf{R}_{y,\gamma}$ : rotation matrix about y-axis with yaw angle

$\mathbf{R}_{z,\psi}$ : rotation matrix about z-axis with roll angle

$s$ : sine

TMJ: temporomandibular joints

$W_{\max}$ : the maximum protrusion

WY-1: first generation of Waseda Yamanashi robot

$x_D, y_D, z_D$ : values of point D along x, y, z-axes

$z_1$ : the height of the fixed frame on z-axis

$z_2$ : the height of the third joint on z-axis

$\beta_i$ : an angle about z-axis at moving frame platform

$\theta$ : the variable, rotational angle of the actuator

$\lambda$ : an angle about z-axis at fixed platform

$\phi, \gamma, \psi$ : pitch, yaw, roll angles

---

## **Chapter 1: Introduction**

An articulator, which is used to visualize occlusal relationships and enables dentists to work on fitting dental restorations without continual direct contact with the patient, is a mechanical device used in dentistry to which casts of the maxillary (upper) and mandibular (lower) teeth are fixed, reproducing recorded positions of the mandible in relation to the maxilla. Articulators are adjustable to replicate the kinematic topology of the patient's jaw by changing joint locations relative to the frame of reference. Articulators are mainly used for studying individual teeth and full dental arches for diagnosis and treatment planning as well as allowing adjustment of fixed and removable prostheses and indirect dental restorations. Therefore, the objective of the articulator is to produce and reproduce occlusal relationships extraorally [2]. An articulator assists not only in the fabrication of removable prosthodontic appliances, fixed prosthodontic restorations, and orthodontic appliances but also in maxillofacial surgeries as well as oral implantation [1]. Hence, the articulator is the cornerstone requirement for prosthodontics, restorative dentistry, and dental surgery as well as one of the core devices in dental education and research.

### **1.1 Historical background and current devices in practice**

For over 200 years, dentists have been trying to develop methods and devices to duplicate positions and movements of dentition according to the relationship of the human skull. Since unmounted casts give only basic information about the patient's occlusal relationship, copying positions and movements of the jaw is a significant step for achieving a complete analysis of the functional relationships. From the first articulator (slab articulator) to the modern articulator, dentists have developed many instruments to

simulate jaw movements and record jaw positions, which help to maintain casts centrally aligned and in predetermined vertical positions, perform functional analysis of occlusion, pursue occlusal equilibration, and carry out reconstruction of occlusion [3]. Generally, there are four different types of designs of articulators:

- Simple hinge articulator – provides a single hinge without lateral movements. It has one degree of freedom. Two parts of it rotate around the hinge and give the very basic relationship between maxilla and mandible relationship. The simple hinge articulator has limited value in dentistry. It allows a preliminary evaluation of static tooth arrangements on study models or assists discussion with patients [16].

- Average value articulator – has its condylar angle fixed at  $30^\circ$ . It has an adjustable incisal guidance without provision for condylar side shift adjustment. It has 3 degrees of freedom. But its limitation is significant in practice since the condyles' angles are fixed. The average value articulator produces an approximation of condyles' movements and balanced occlusion. [17].

- Semi-adjustable articulator – only allows adjustment of condylar inclination and Bennett angle or progressive side shift in most cases. In this design, intercondylar width is usually fixed with certain width settings. Thus, this articulation is improved based on the average value articulator. However, in this articulator, the simulated TMJ is mechanically simplified and it does not produce certain condylar movements. The articulators, both arcon, and nonarcon, allow realistic approximation of anatomical relationships of teeth and the arch form of articulated casts, condylar relationships, and intercondylar distance. However,

raising the height of its pin without using a hinge axis face-bow transfer would increase the vertical dimension of occlusion, which in turn will create errors.

- Fully adjustable articulator – is designed to duplicate TMJ joints' features with a series of condylar adjustments, plus it allows curved condylar translation paths. Having its 6 degrees of freedom, it can fully duplicate the jaw movements and provides the most accurate duplication of mandible relationships among those articulators. But the complexity of the device such as complicated condylar adjustments and technique-sensitivity makes it unpopular in dental practice.

The articulators mentioned above are most common in clinical practice, education, and studies. However, in addition to their shortcomings discussed above, all of those articulators are passive devices, which need manual adjustment as well as special dental training. The use of a passive mechanical device to replicate active jaw motions is inherently limited, and leads to a trial-and-error approach to fitting and adjusting dental work.

## **1.2 Developments in dental engineering**

Since the early 1990s, there have been many attempts at developing masticatory robots for the purposes of providing dental patient training, jaw simulation, food texture assessment and speech therapy. Some other jaw movement robots which can simulate human mandible movement and reproduce jaw force were applied in various sub-disciplines. Alemzadeh et al. [4] developed a dental test simulator based on the Stewart platform, Bristol parallel robot, used for experiments on dental component materials by simulating human chewing. The research describes an artificial jaw and compliance of the Stewart platform [29], which has 6 degrees of freedom (DOF). Its mechanism and the six

electric actuators, which are altered to match them more closely to the jaw's dynamics by using inner-outer loop control and composite measurements, have very different dynamics by emulating the muscles responsible for the jaw movements. Basically, this is designed to simulate the wear of dental components (i.e., individual teeth, crowns or a full set of teeth). Callegari et al. [5] proposed a 3-PUU (prismatic/universal/universal) parallel mechanism used to perform dental disease pathology research in jaw motion. The design of a mechatronic articulator was intended to be used as a diagnostic and therapeutic instrument for the study of chewing disorders. However, the design is only limited with its computer design architecture and VR simulation. In 1986 the Takanishi laboratory had developed a mastication robot called WY (Waseda Yamanashi) for patients' mouth opening training. Compared to conventional mouth opening devices used in clinical practice such as bite blocks, and wooden screws, which are limited to open the mouth vertically without any sensors, actuators, and control systems, the 6-DOF robot can assist dentists with the quantitative force data to open a patient's mouth with sensors, mechanical actuation, and control systems. Takanishi had developed a 6-DOF parallel robot based on his previous systems, WY-3RIII [10], which had fewer degrees of freedom, with the considerations of pathological and abnormal movements of the human jaw. There were many improvements in this project, such as it has more degrees of freedom, patients feel safe while it is under patients' control with a safety button, the additional sensors prevent the mandible from tightly gripping the mouth opening gage, the electrical stopper with fuses protects patients from excessive mouth openings, and the feedback system reduces the error as small as possible, etc. [6]-[9]. This team also developed a mastication robot for the purpose of measuring the efficiency of mastication and its quantification experimentally, which is a

mechanical simulator based on human mastication anatomy. The robot has four subsystems: 1. A human skull-shaped frame; 2. The actuator system has nine artificial muscle actuators mimicking human mastication muscles; 3. Sensors are force sensors for each actuator and micro pressure sensors for molars; 4. The closed-loop control with sensor feedback. The advancement of the robotic system is that not only can the efficiency of the mastication be measured and quantified but the shape of artificial teeth can be altered to be suitable for biting motions in various trajectories of the mandible in regard to mastication efficiency [10]. There are other robotic models of the mastication systems developed for food industries' testing purposes [11]-[14]. Xu et al. made a mastication robot based on the mastication robot WY's design and improved it by changing the platform like mandible being a moving plate and the skull a ground plate. Thus its measurement of chewing efficiency was closer to the human jaw [14]. Those robots discussed above can simulate human jaw movement though, they are not developed for duplicating individual patients jaw positions and movements.

### **1.3 Virtual Articulator**

Since the first digital image was obtained of the bite registry, of the global dental arch, and of the surfaces of each tooth, Kordass and Gartner described the programming and adjustment methods of the virtual articulator in 1999 [21]. Using a 3D laser scanner and a digital camera, the processed data were ready to use by the scanner software and for on-screen visualization and digitalized manipulation [22]. Complete with an ultrasound system and optoelectronic device, this yielded room for detecting and recording mandibular movements [22]-[23]. Therefore, current technology allows to navigate and view the world in 3D, and dentistry is no different. Using computer-aided design (CAD)



systems and reverse engineering tools enables analysis of the kinematics of jaw movements in virtual reality (VR). Not only can the virtual articulator significantly reduce the limitations of the mechanical articulator, but it allows dentists to analyze static and dynamic occlusions as well as jaw relationships [18]. The virtual articulator, which is completely adjustable and mathematically simulated, is capable of simulating jaw movements, by enabling correction of the VR occlusal surface and moving VR occlusal surfaces of teeth against each other to yield smooth and collision-free movements [19],[20].

#### **1.4 Summary and Drawbacks**

Presently, much of technical dental work uses the wax-up technique to construct the framework, and then the design work finishes with hand applied ceramic veneer, using a mechanical articulator that attempts to duplicate the jaw movements and interarch jaw relationships [25]; other ceramic frameworks are largely done with CAD/CAM. Even though the virtual articulator is popular in routine practice to diagnose and simulate the functional effects upon dental occlusion, this mechanical scenario is different from real biological settings and causes serious problems. The technical procedure greatly reduces the accuracy of reproduction such as measuring facial dimensions and accounting for muscular influence due to patient anxiety. Mounted models cannot represent the actual dynamic conditions of the occlusion in the mouth; approximation of passive movements leads to misdiagnosis [19]. Moreover, those robots which simulate jaw movements are developed for other purposes as mentioned above. None of them can be used in clinical practice for reproducing the position and movements of the jaw, because of the complexity and variety of every individual patient's jaw movement patterns. In addition, the virtual

articulator upgrades the level of accuracy and creates high-quality communication between the dentist and dental technician, though it is limited to the digital world. Since the human oral cavity is a very sensitive environment (even a tiny hair in the mouth can cause discomfort), the basic errors, the reproduction of dynamics, excursive contacts of physical models and dental work seem to lower the reliability. Therefore, the usefulness of the virtual articulator on dental prosthetics still needs to be explored.

## Chapter 2: Notion of the Idea

As A. Gysi, the genius and pioneer of modern prosthetic dentistry, emphasized in 1907, the problem of articulation could only be solved when dentistry succeeded to record and reproduce jaw movements of individual patients [3]. However, the use of a passive mechanical device to replicate active jaw motions is inherently limited and leads to a trial-and-error approach to fitting and adjusting dental work. An alternative to the existing trial-and-error workflow would involve the digital capture of actual patient-specific jaw motion, and replication of that motion using a robotic articulator. In this way, one could be sure that the motion of the articulator accurately represents the working conditions that would be experienced by dental prostheses, to within the combined accuracy of the motion capture, the kinematics of the robot, and the fidelity of the dental model in which the prosthesis is tested. Scaling of the captured motions would also allow for compensation of dimensional stability issues commonly encountered when working with models. This workflow is represented in Figure 2.1.

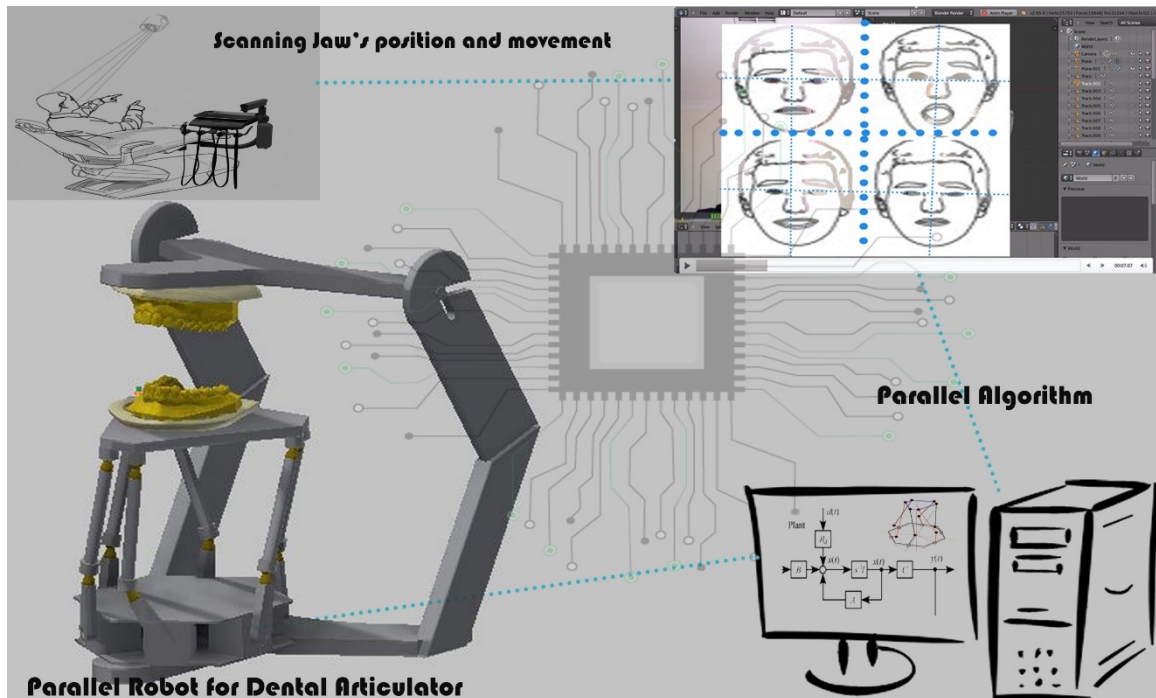


Figure 2. 1 Robotic Dental Articulator Concept

The work presented here is an attempt to solve the problem by tracking individual patients' jaw movements with a tracking system (details on motion tracking are outside the scope of this thesis) and copying these to the articulator with a parallel robot structure, which moves like a human mandible and on which the patient's casts can be attached. This can not only solve the traditional problem in dentistry but also has the following benefits:

- Increase accuracy. Since patients tend to be anxious about interventions in the maxillofacial area, this greatly affects the process of measurement and decreases the accuracy due to abnormal jaw movements. The new device would record jaw movement naturally during the conversation and relaxed interactions with the patient.
- Provide precise repetition of movements and position. Once an individual patient's jaw movements are recorded, dentists can repeat the patient's protrusive and lateral movements as well as a centric relation (CR) on the dental model many times, even

introducing realistic motion perturbations if desired, without considering fatigue of the jaw, which would otherwise decrease the accuracy. This is a significant advancement in clinical practice.

- Record and compare pre- and post-intervention mandible movements. Since the robot can be programmed and controlled easily with the data before or after a patient's visit, it can significantly shorten the dentist chair-side time and also contribute to the accuracy of dental work.
- Analyze static and dynamic occlusions as well as gnathic and joint conditions.
- Possible to introduce and/or modify new settings according to the patient and assist with patient education.
- Add a new dimension, a dynamic motion, to the study of anatomy, pathology, and methods of dentistry for treatment and education purposes.

In this project, a parallel robot is presented to serve as an active dental articulator. Because the jaw moves in six degrees of freedom (DOF) but the ranges of motion in these DOF are highly dissimilar, the robot is optimized for kinematic performance specifically within the typical range of motion used in dental articulation. This results in an asymmetric robot configuration (although the topology of each leg is the same, the dimensions are different) as described in more detail in the following chapters.

## Chapter 3: Approach

Defining the characteristics of the human jaw and its movement is the first step for modeling the parallel robot, and then based on the jaw's workspace the robot is optimized.

### 3.1. Workspace and Movements of the Human Mandible

The jaw is often modeled as a simple hinge; an example is the robot WY-1, which has 1-DOF [6]. Although the primary open/close motion of the jaw is similar to a simple hinge, the relative motion between the upper and lower jaws is more complex and has components in all six DOF.

#### 3.1.1 Functional Anatomy of Masticatory System

“Nothing is more fundamental to treating patients than knowing the Anatomy,” as Jeffrey P. Okeson said to highlight the importance of the functional anatomy of the mastication system [15]. The following anatomic components make up the basic functional structure of the mastication system.

1. *Human dentition and its supportive structures.* The dentition of an adult is made up of 32 permanent teeth, and the supportive structures include gingiva, periodontal ligament, cementum, and alveolar bone.

2. *Skeletal components* are the maxilla (developmentally two maxilla bones are fused at the midpalatal suture), the mandible, a U-shaped bone, and the temporal bone, which has important anatomical structures such as mandibular fossa, articular eminence etc.

3. *The temporomandibular joint (TMJ)*, which is a core part of all jaw movements and one of the most complex joints in human body. The main components of TMJ are the joint

capsule, mandibular condyles, articular disc, the temporal bone's articular surface, stylomandibular ligament, sphenomandibular ligament, temporomandibular ligament, and lateral pterygoid muscle.

4. *The ligaments.* Ligaments act as passive restraining devices to limit and restrict border movements in order to protect other structures; they do not enter actively into joint function though. There are three functional ligaments supporting the TMJ (collateral ligaments, the capsule ligaments, and the TMJ ligaments) as well as two accessory ligaments.

5. *The muscles of mastication.* The main functions of skeletal muscles are support and movement. The muscles of mastication move the jaw and hold its position. There are four pairs of mastication muscles: the masseter, the temporalis, the medial pterygoid, and the lateral pterygoid. The digastric muscles also play a significant role in moving the mandible as well as other functions, even though they are not considered as muscles of mastication [15].

### 3.1.2 Border and Functional Movements of Human Mandible

Jaw movements occur as a complex series of interrelated 3D rotational and translational actions. While four groups of muscles drive the jaw to perform complex movements, special anatomical and physiological features of the TMJ determine the trajectory of the movements relative to the maxilla. Basically, the TMJ regulates and constrains a complex series of interrelated rotational and translational jaw movements. Since there are two TMJ joints, bilateral synovial articulation between temporal bone and mandible, connected

through the jawbone, the movements are combinations of simultaneous activities of both. Rotational movements occur on axes in the horizontal, frontal and sagittal reference planes within the condyles, and translational movements occur between the superior surface of the articular disc and the inferior surface of the articular fossa, resulting in very complicated movements, such as depression, elevation, lateral deviation, protrusion and retrusion as illustrated in Fig. 3.1.



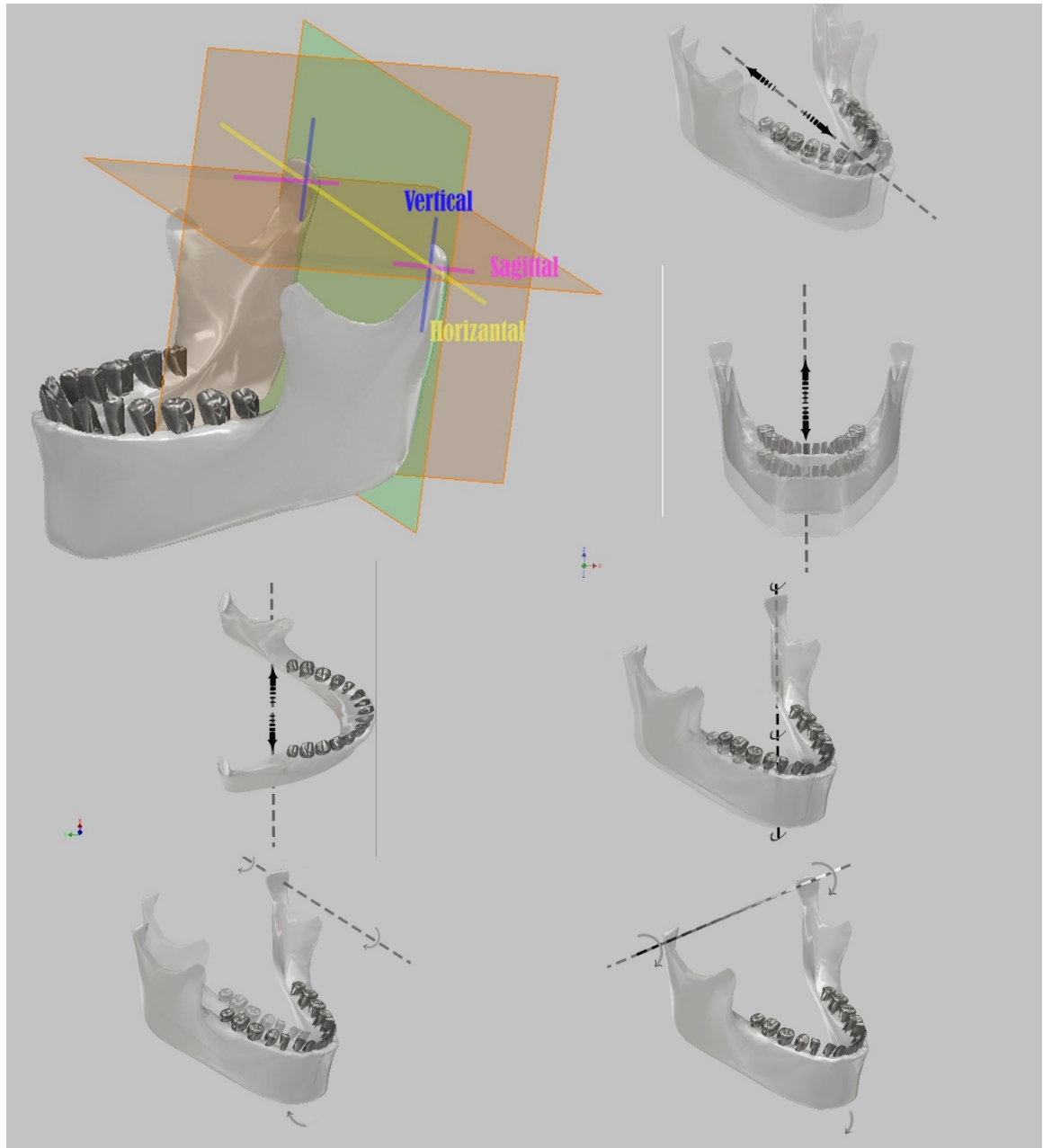


Figure 3. 1 Movement of Mandible

### 3.1.2.1 Sagittal Plane Border and Functional Movements

Basically, there are four distinct movements when mandible motion is viewed in the sagittal plane: posterior opening border, anterior opening border, superior contact border, and functional movements as seen in Fig. 3.2. (1) Posterior opening border movements

occur when the mandible rotates about the horizontal axis to a distance of 20-25 mm between the upper and lower incisal edges (first stage), then the condyles translate and the axis of rotation of the mandible shifts into the bodies of rami (second stage) and the condyles move anteriorly and inferiorly while the anterior portion of the mandible is moving posteriorly and inferiorly. The maximum range of opening is about 40-60 mm between incisal edges. (2) Anterior opening border movements. In these movements, the eccentricity is produced by the posterior movements of the condyles from the maximally open position of the mandible where the condyles are at the most anterior position. (3) Superior contact border movements are determined by the characteristics of the occlusion surfaces of the teeth. (4) Functional movements usually take place within the border movements during the functional activity of mandible.

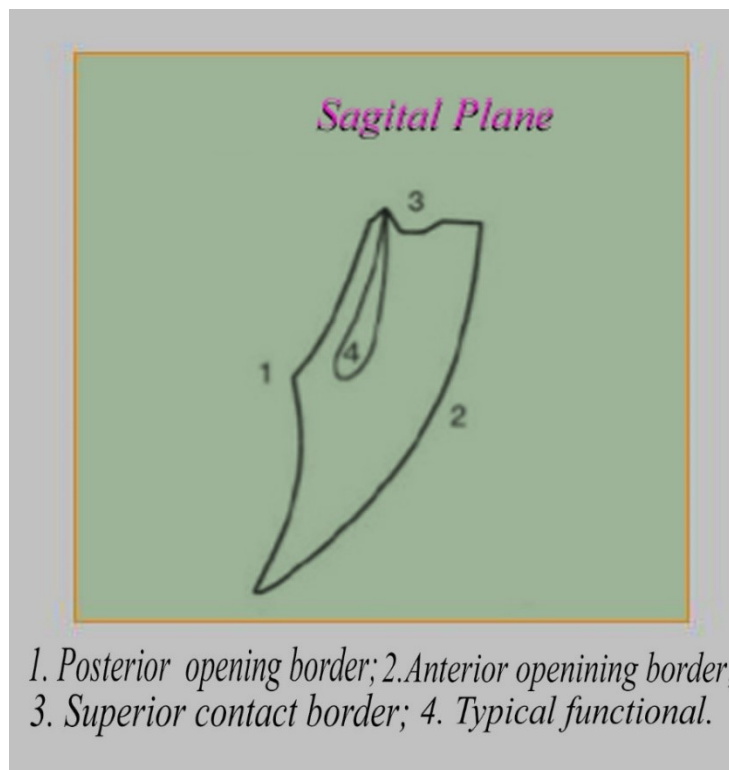


Figure 3. 2 Border and Functional Movements in Sagittal Plane

### 3.1.2.2 Horizontal Plane Border and Functional Movements

Viewing in the horizontal plane, four distinct movements that form a rhomboid pattern can be seen as in Fig. 3.3. The four movements are left lateral, right lateral, continued left lateral border with protrusion, and continued right lateral border with protrusion movements. The movements occur when the mandible is rotating around one condyle and the other condyle is orbiting a vertical axis through the first condyle simultaneously while the mandible midline is being moved back to coincide with the midline of the face by anterior and opposite movement of the rotational condyle.

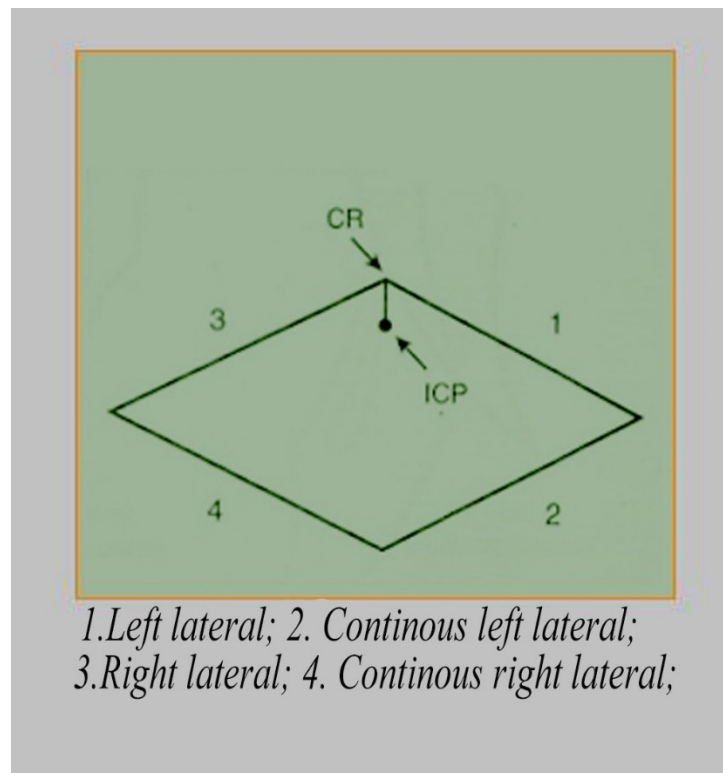


Figure 3. 3 Border and Functional Movements in Horizontal Plane

### 3.1.2.3 Frontal Border and Functional Movements

A shield-shaped pattern can be seen when viewed in the frontal (vertical) plane. The mandibular motion has four distinct movement components: left lateral superior border, left lateral opening border, right lateral superior border and right lateral opening border. Those movements occur when the condyles move in a lateral convex path with inferior movements of one or two condyles simultaneously as illustrated in Fig. 3.4.

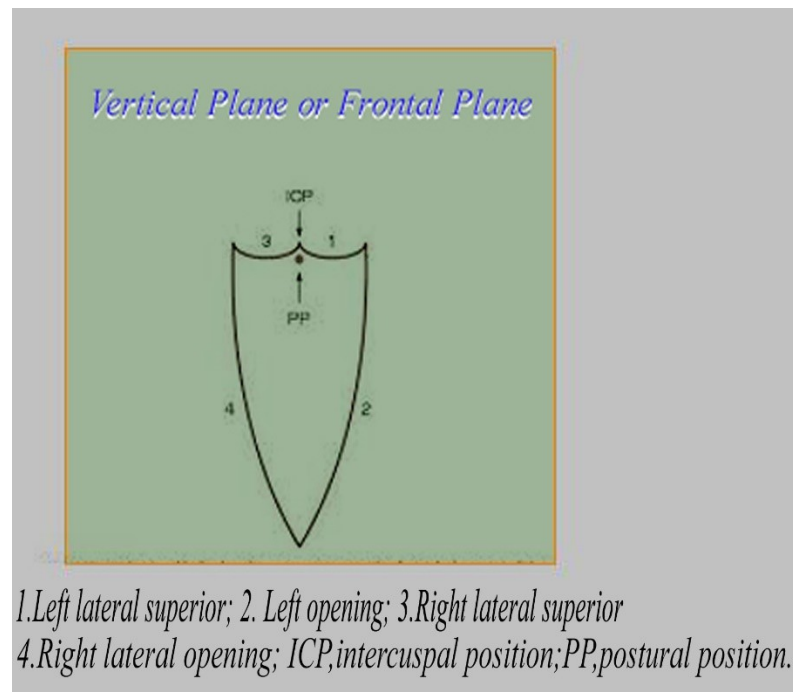


Figure 3. 4 Border and Functional Movements in Frontal Plane

By combining those three plane mandibular movements, a 3D envelope of motion or mandibular workspace can be created as in Fig. 3.5

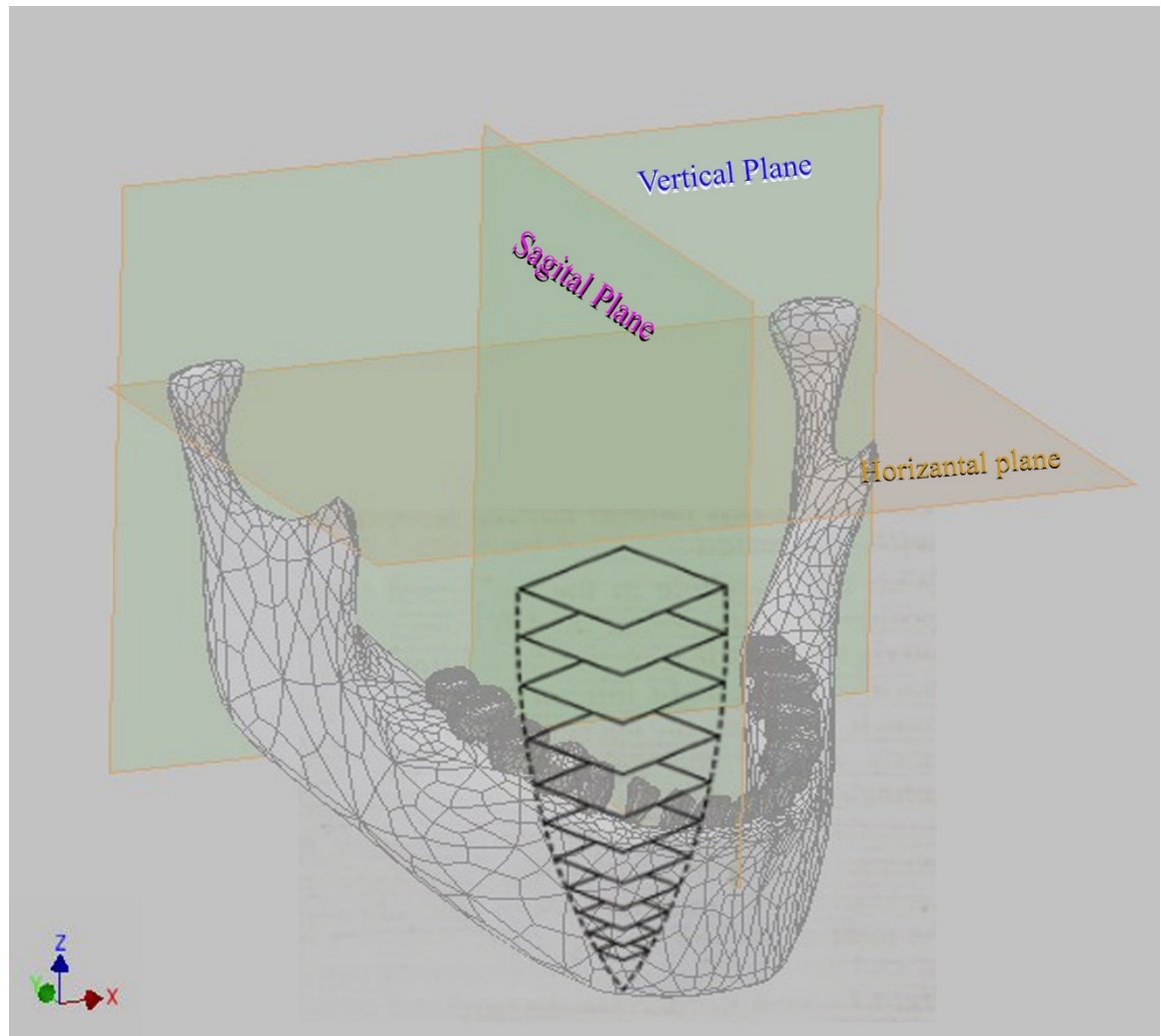


Figure 3. 5 Envelope or Workspace of the Mandible in 3 Dimensional Space

Therefore, the arbitrary combinations of two condyles' lateral, anterior or posterior, and superior or inferior movements create the border of mandible three-dimensional movements which is the ultimate purpose of our design. Accounting for the interference of dentitions with these movements as well as other non-natural movements, we consider the movement of the jaw as a 6-DOF system [15].

This is recognized in the multi-jointed structure of passive articulators [2]. Therefore, a robotic dental articulator should allow small translation motions in all three directions as

well as small rotations about both axes normal to the main “hinge,” in addition to the obvious gross motion. The design requirements must be set based on the trajectory of the mandible in its border movements or workspace.

### 3.2. 6-RSS Architecture for Dental articulator

The chosen architecture is a 6-RSS parallel robot, as shown in Figure 3.6. This leg type is chosen mainly because small, inexpensive servomotors are readily available to serve as the actuators. An obvious alternative would be the 6-SPS (Stewart platform) architecture, but it is desirable to avoid linear actuators, as they tend to be difficult to miniaturize to the size scale needed for a dental articulator.

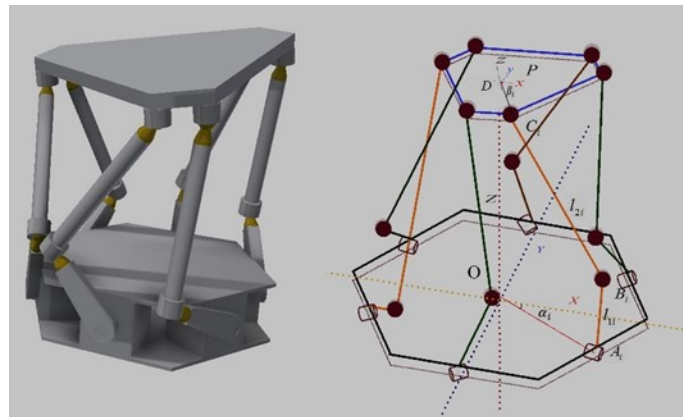


Figure 3. 6 6-RSS Architecture for Dental Articulator

The 6-RSS parallel robot, as its name implies, has six legs connecting fixed and moving platforms, each leg having a revolute and two spherical joints to connect the leg segments  $l_{1i}$  and  $l_{2i}$ . It consists of six revolute joints at points  $A_i$  on the fixed base (where subscript  $i$  represents the  $i^{\text{th}}$  leg, from 1 to 6), six spherical joints at  $B_i$  between first links  $l_{1i}$  and second links  $l_{2i}$ , and six spherical joints at  $C_i$ , which connect second links  $l_{2i}$  and the end effector. The base is fixed and considered static and the end effector moves in the workspace based

on the robot's kinematics. The revolute joint rotates about its axis and has one degree of freedom. The spherical joint rotates in pitch, yaw and roll through the center of its sphere, and has three degrees of freedom. Based on the Chebyshev-Grübler-Kutzbach [27] criterion for mechanism mobility, the formula is given, in this case, by

$$F = \lambda (n - j - 1) + \sum_i f_i - f_p \quad (1)$$

in which

$F$  = degrees of freedom of the robot

$\lambda$  = degree of freedom in the space (i.e., 6 for spatial motion, 3 for planar motion)

$n$  = the number of links in the manipulator including the base

$j$  = the number of binary joints of the mechanism

$f_i$  = degree of relative motion permitted by joint  $i$

$f_p$  = the total number of passive degree of freedom

Thus, we can have  $\lambda = 6$  for the motion space of the robot, and the number of links including the base is  $n = 6 + 6 + 2 = 14$ . There are six binary revolute joints at  $A_i$  ( $j_1 = 6$ ), and also  $6 \times 2 = 12$  spherical joints at  $B_i$  and  $C_i$  ( $j_3 = 12$ ). Moreover, for each RSS kinematic structure there is one passive degree of freedom (rotation of the link between each pair of spherical joints about its long axis, not contributing to overall robot motion), and therefore,  $f_p = 6$ . Then, applying the Chebyshev-Grübler-Kutzbach criterion, the degree of freedom of this robot can be calculated as follows:

$$F = 6(14 - 18 - 1) + (12 \times 3 + 6) - 6 = 6 \quad (2)$$

This parallel robot produces a complete spatial movement with three degrees of freedom for position and three degrees of freedom for orientation. There is no actuator redundancy in this case, since the number of actuators is also equal to the degrees-of-freedom of the robot [27].

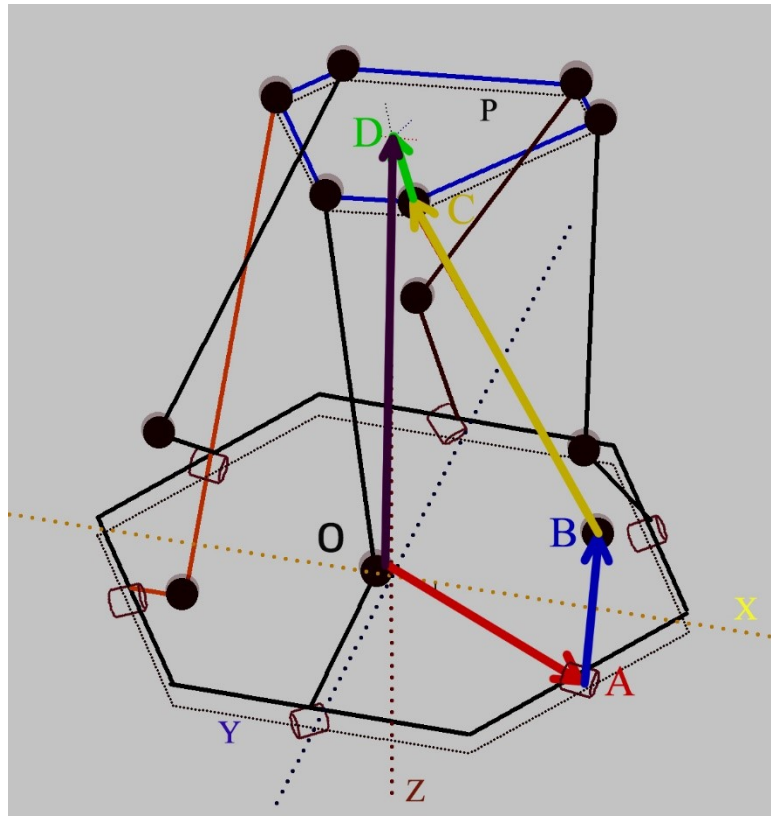


Figure 3. 7 Vector-Loop Closures

The fixed platform is designed as a hexagon shape, called the base, while the moving platform is called the end effector. These two bodies are coupled by six legs with the upper and lower segments  $l_{1i}$  and  $l_{2i}$  attached by spherical joints at  $B_i$ , and each leg connected to the end effector at  $C_i$  with spherical joints and to the fixed platform at  $A_i$  with revolute joints. As shown in Fig. 3.7, the pose of the moving platform relative to the base is defined by a position vector  $D$ . In this figure, the closure of each kinematic loop can be expressed in the vector form as



$$\overline{OD} = \overline{OA} + \overline{AB} + \overline{BC} + \overline{CD} \quad (3)$$

in which interchangeable notations  ${}^0\mathbf{D} = \overline{OD}$ ,  ${}^0\mathbf{A} = \overline{OA}$ ,  ${}^0\mathbf{B} = \overline{OA} + \overline{AB}$ ,  ${}^0\mathbf{C} = \overline{OA} + \overline{AB} + \overline{BC}$  are used in the equations in the following chapters.

### 3.3. Inverse Kinematics

The pose of the end effector is expressed as a position vector  ${}^0\mathbf{D} = [x_D \ y_D \ z_D]^T$  and a set of Euler angles  $[\phi \ \gamma \ \psi]^T$ . For inverse kinematic analysis, the pose of the end effector is given and the problem is to find the joint variables of the manipulator,  $\theta = [\theta_1, \theta_2, \theta_3, \theta_4, \theta_5, \theta_6]^T$ . For a given pose of the end effector, the inverse kinematics of each “generic” leg can be solved separately. Denoting the center point of the revolute joint of the leg as  ${}^0\mathbf{A}$ , its connection to the first spherical joint as  ${}^0\mathbf{B}$ , and its connection to the second spherical joint as  ${}^0\mathbf{C}$ , all of these referenced to the global reference frame O located at the center of the fixed platform, and the local end-effector reference frame P with its location denoted as  $\mathbf{D}$ , the position solution of the leg in Fig. 3.8 is as follows. From the geometry of the manipulator, the point  ${}^0\mathbf{C}$  is expressed in the global reference frame as

$${}^0\mathbf{C} = {}^0\mathbf{D} + \mathbf{R}_{x,\phi} \mathbf{R}_{z,\psi} \mathbf{R}_{y,\gamma} {}^P\mathbf{C} \quad (4)$$

where  $\mathbf{R}$ s are standard rotation matrices and P denotes the local reference frame of the end effector. Then,

$${}^0\mathbf{C} = {}^0\mathbf{D} + \begin{bmatrix} c\gamma c\psi & -s\psi & s\gamma c\psi \\ c\phi c\gamma s\psi + s\phi s\gamma & c\phi c\psi & c\phi s\gamma s\psi - s\phi c\gamma \\ s\phi c\gamma s\psi - c\phi s\gamma & s\phi c\psi & s\phi s\gamma s\psi + c\phi c\gamma \end{bmatrix} {}^P\mathbf{C} \quad (5)$$

where  ${}^P\mathbf{C} = [r_2 c\beta \ r_2 s\beta \ 0]^T$ , and  $r_2$  and  $\beta$  define the location of C in frame P.

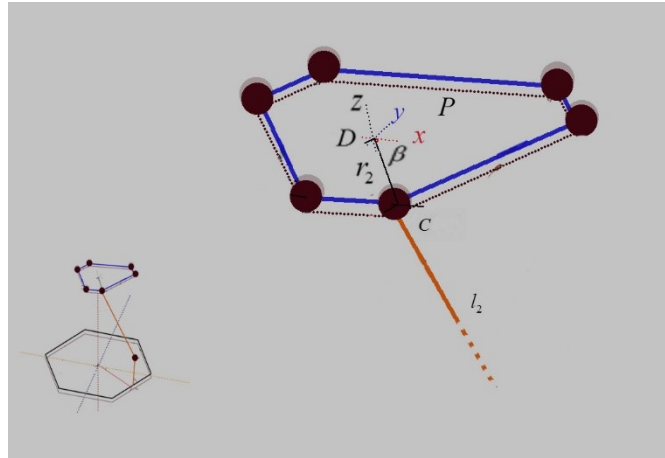


Figure 3. 8 The End Effector of the Robot

This yields  ${}^0\mathbf{C}$  as follows.

$${}^0\mathbf{C} = \begin{Bmatrix} P \\ Q \\ S \end{Bmatrix} = \begin{bmatrix} x_D - r_2 s \beta s \psi + r_2 c \beta c \gamma c \psi \\ y_D + r_2 c \beta (s \phi s \gamma + c \phi c \gamma s \psi) - r_2 c \phi c \psi s \beta \\ z_D - r_2 c \beta (c \phi s \gamma - c \gamma s \phi s \psi) + r_2 c \psi s \beta s \phi \end{bmatrix} \quad (6)$$

The position of  ${}^0\mathbf{B}$  can be found by using Denavit-Hartenberg parameterization with the notations in Fig. 3.9, with  $\theta$  as the variable.

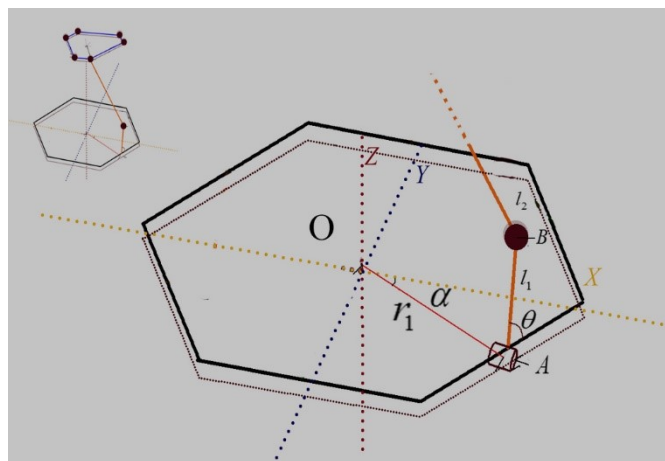


Figure 3. 9 Base Frame

$${}^0\mathbf{B} = {}^0\mathbf{T}[0 \ 0 \ l_1 \ 1]^T = \begin{bmatrix} ca & -sac\theta & sas\theta & r_1c\alpha \\ sa & cac\theta & -cas\theta & r_1s\alpha \\ 0 & s\theta & c\theta & 0 \\ 0 & 0 & 0 & 1 \end{bmatrix} [0 \ 0 \ l_1 \ 1]^T \quad (7)$$

Then,

$${}^0\mathbf{B} = \begin{Bmatrix} K \\ M \\ N \end{Bmatrix} = \begin{bmatrix} l_1sas\theta + r_1c\alpha \\ -l_1cas\theta + r_1s\alpha \\ l_1c\theta \end{bmatrix} \quad (8)$$

where  $r_1$  and  $\alpha$  define the location of **A** in frame **O**, and  $l_1$  is the length of the lower leg. Since  $l_2$  is the upper leg length between points **C** and **B**, we can derive an equation for  $\theta$ , in terms of the parameters above, as follows:

$$l_2 = (\| {}^0\mathbf{C} - {}^0\mathbf{B} \|) = [(P - K)^2 + (Q - M)^2 + (S - N)^2]^{1/2} \quad (9)$$

Defining

$$H = P^2 + Q^2 + S^2 + r_1^2 + l_1^2 - l_2^2 - 2Pr_1c\alpha - 2Qr_1s\alpha$$

$$h_1 = l_1Qca - l_1Ps\alpha$$

$$h_2 = l_1S$$

(10)

Then,

$$2h_1s\theta - 2h_2c\theta + H = 0 \quad (11)$$

This is the generic equation for solving the input angle,  $\theta$ , of each leg. Once the position vector of the end effector is given, the desired input angle  $\theta$  can be solved numerically in MATLAB.



Therefore, it is necessary to optimize the parameters  $l_{1i}$ ,  $l_{2i}$ , where  $i = 1 \dots 6$  based on the border movements of the jaw. Based on a symmetric robot (plane of symmetry equivalent to the sagittal plane passing through the center of the head), the data of the trajectory of the lower incisor point of the mandible measured by using a mandibular kinesiograph, the main parameters of the envelope of the lower incisor point are as follows [26]:

The maximum mouth-opening movement  $L_{\max} = 42.6$  mm

The maximum protrusion  $H_{\max} = 12.2$  mm

The maximum lateral movement  $W_{\max} = 30.0$  mm.

Based on these functional requirements, we set a range of motion of  $\pm 15$ mm in the x-direction (symmetric based on  $W_{\max}$ ),  $-12$ mm to  $+2$  mm in the y-direction (based on protrusion of 12 mm and retraction of 2 mm), maximum displacement of 60mm in the z-direction (values for the range of motion vary based on the links values as illustrated in Fig 4.2),  $\pm 17$ deg rotation about the z-axis,  $\pm 11$ deg rotation about the y-axis, and 0 to 31deg rotation about the x-axis. This can be thought of as a 6-dimensional hypercube of workspace.

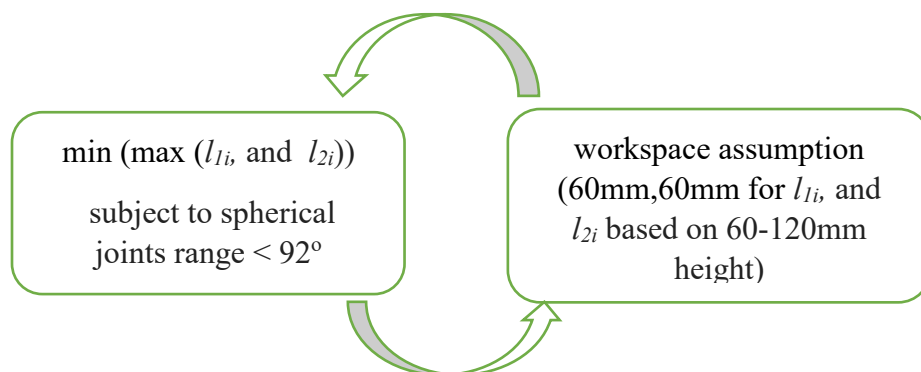


Figure 4. 1 Workspace Assumption

The optimization problem is stated in Figure 4.1. Here, it is necessary to optimize initial values of  $l_{1i}$  and  $l_{2i}$  first. Based on physical limitations of hardware, there are some constraints in this design, such as the range of servos' revolute angles between  $25^\circ$ - $160^\circ$  as well as the maximum range of spherical joint motion of  $92^\circ$ , as in Fig. 4.2.

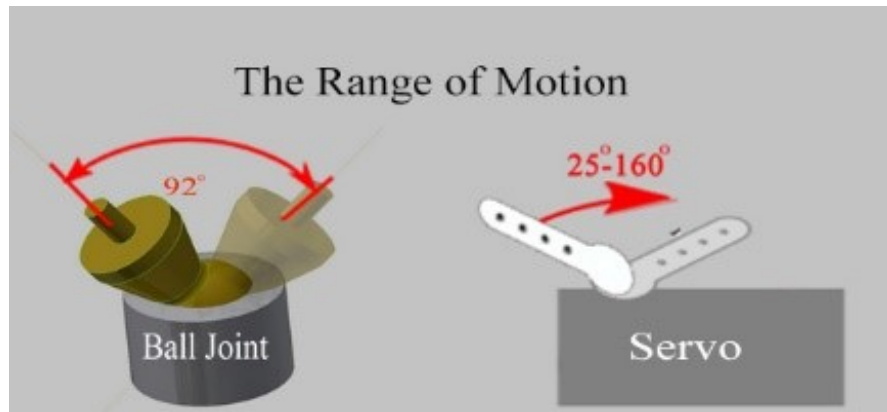


Figure 4. 2 the Maximum Range of Motion

To avoid impractical joint angle values, the optimization limited the spherical joints to a range of 92 degrees total motion and the maximum motion angle of the end effector of  $31^\circ$ . Moreover, the maximum height of opening,  $L_{\max}$ , equals the difference of  $L_1$  and  $L_2$  as illustrated in Fig 4.3.

$$L_1 - L_2 \geq 60 \text{ mm} \quad (12)$$

$$l_{1i} + l_{2i} - (l_{2i} - l_{1i} \cos 92^\circ) \geq 60 \text{ mm} \quad (13)$$

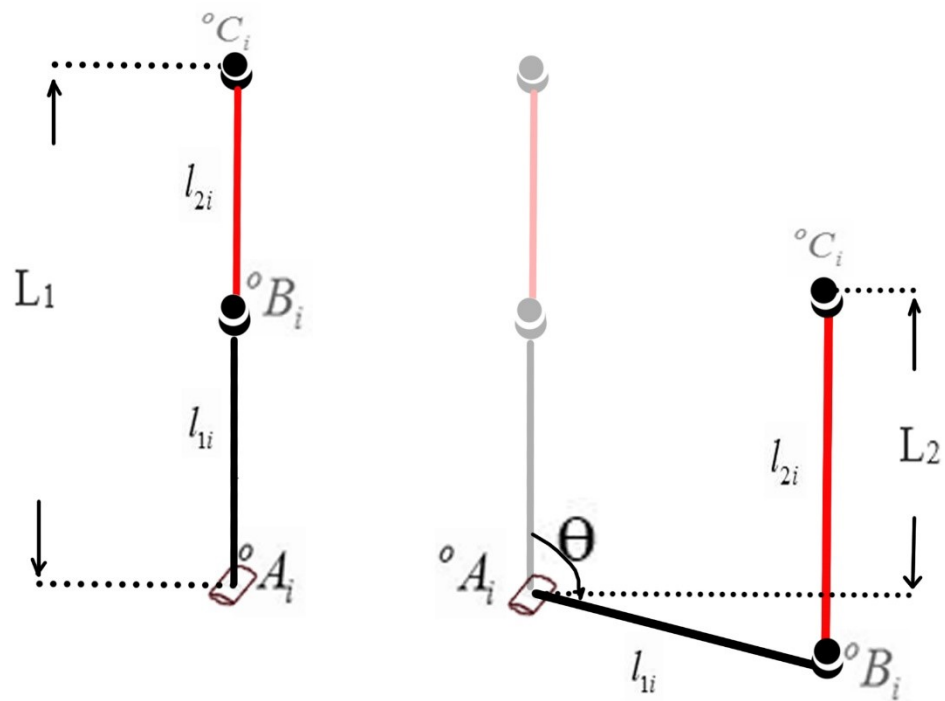


Figure 4. 3 Initial Optimization of First and Second Leg

We can derive an approximate value for  $l_{1i}$  from the equation above, which is 60 mm and we assume  $l_{2i} = 60$  mm. Therefore, the range of motion along the z-axis will be 60 mm to 120 mm in the first iteration. Hence, accounting for the given initial values of  $l_{1i}$  and  $l_{2i}$ , the set of points within the workspace where the robot is supposed to reach can be simulated by using the “ndgrid” function in Matlab as “[x,y,z]=ndgrid(-15:3:15,-2:3:12,60:6:120).”

Defining initial values ( $l_{1i} = 60\text{mm}$  and  $l_{2i} = 60\text{mm}$ ) for the optimization, we derive values of angles for each leg respectively by the inverse kinematics with the data of the vectors that we produced as grid vectors, solving the inverse kinematics by using the fzero function in Matlab based on the equations derived in the previous chapter. Then, using the angles and the corresponding vector points, the values of the vector  $\|AC\|$  can be obtained.



Based on the  $\|AC\|$  values, we optimize for new values for the links of every single leg respectively by using equations (14) and (15).

$$l_{1i} = (\|AC\|_{\max} - \|AC\|_{\min}) \quad (14)$$

$$l_{2i} = \|AC\|_{\max} - l_{1i} \quad (15)$$

Then, using average values of new and old  $l_{1i}$  and  $l_{2i}$ , this process is iterated until  $l_{1i}$  and  $l_{2i}$  values converge. The flowchart of the process is illustrated in Fig. 4.4.

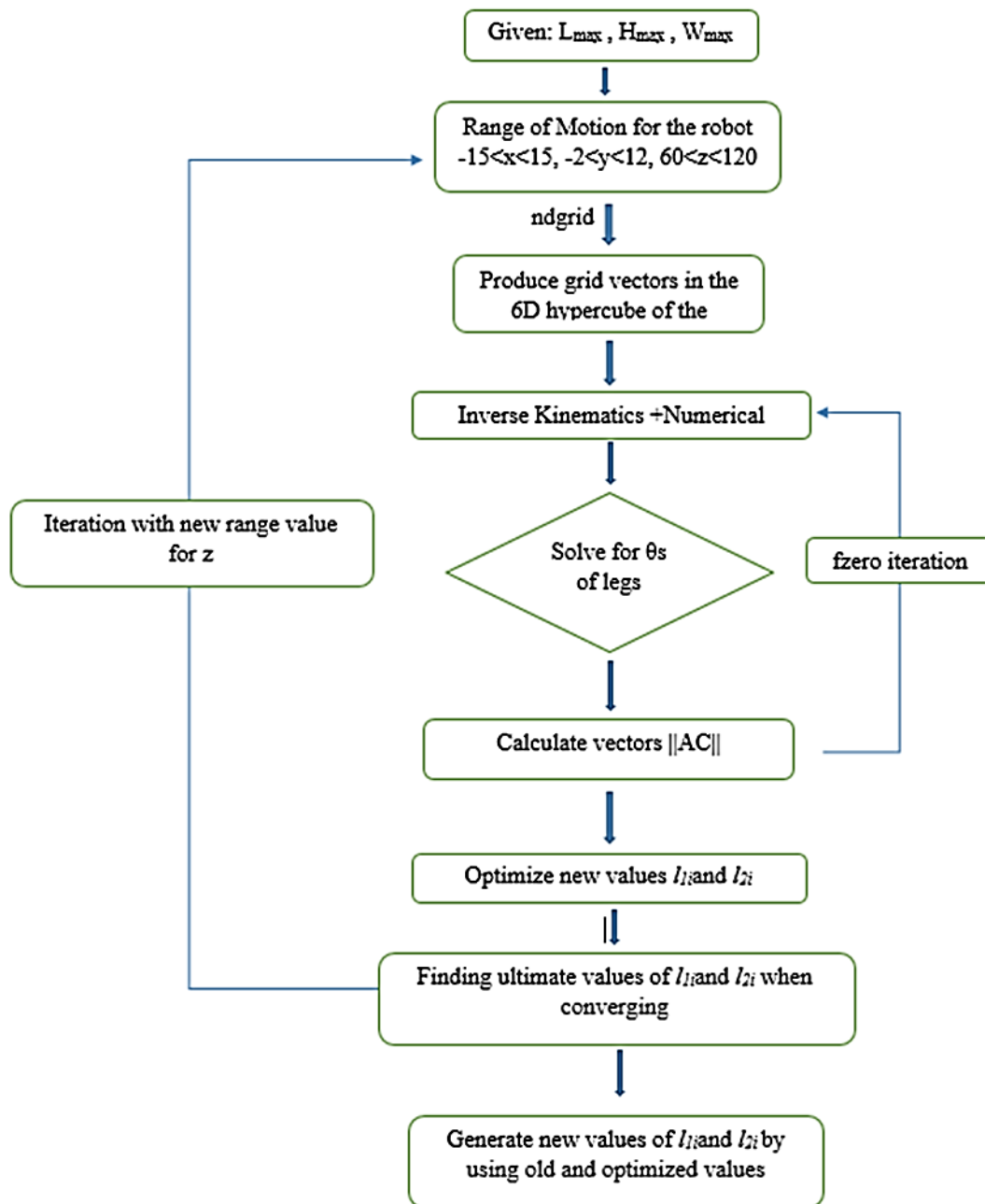


Figure 4. 4 Flowchart of the Optimization Process

After 8 iterations of this process, the values of  $l_{1i}$  and  $l_{2i}$  have converged to the values given in Table 4.2.

Table 4. 2 Iterations and  $l_{1i}$  and  $l_{2i}$  Values (mm)

iterations	$l_{11}$	$l_{12}$	$l_{13}$	$l_{21}$	$l_{22}$	$l_{23}$
initial	60	60	60	60	60	60
2	91.5271	86.0047	80.3709	72.8352	54.5726	56.9260
3	91.1801	86.3433	82.1293	70.1212	59.3213	47.0838
4	91.1801	86.3433	82.1293	70.1212	59.3213	47.0838

Hence, the above flowcharts were implemented in MATLAB to find the leg length parameters which allow reaching all poses in the workspace hypercube while maintaining minimum robot size (as measured by the longest leg).

The robot design resulting from the optimization process described above is shown in Fig. 4.5. The leg parameters are given Table 4.3.

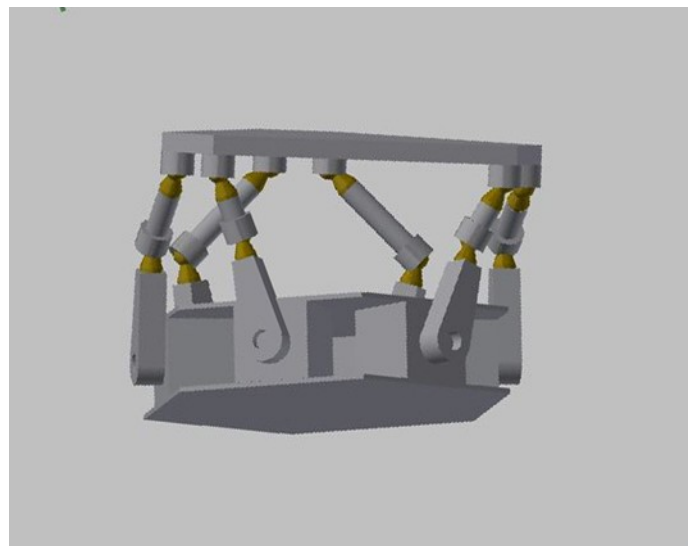


Figure 4. 5 CAD Model of Optimized Robot

Table 4. 3 Optimized Legs' Length Parameters

Leg	$l_{1i}$ (mm)	$l_{2i}$ (mm)
1	91.1801	70.121
2	86.3433	59.3213
3	82.1293	47.0838

## Chapter 5: Physical Design

### 5.1 Mechanical Components

The CAD model of the robot has been done with Autodesk Inventor. When it comes to making its physical model, there are a couple of challenging issues, including size and weight of the ball joints. Since commercially available ball joints are made of metal and the size is relatively large, this not only creates bigger inertia than desired but also may reduce range of motion. Therefore, it was decided to create a custom design. Spherical beads were connected with metal rods using glue to achieve the targeted leg lengths as illustrated in Fig. 5.1.

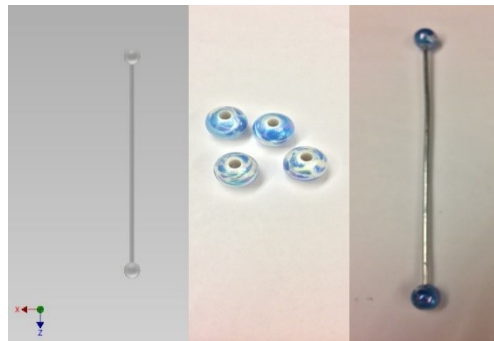


Figure 5. 1 Second Link of The Leg ( $l_{2i}$ )

Other parts of the robot are printed as designed in CAD and are shown in Fig. 5.2 and Fig. 5.3.

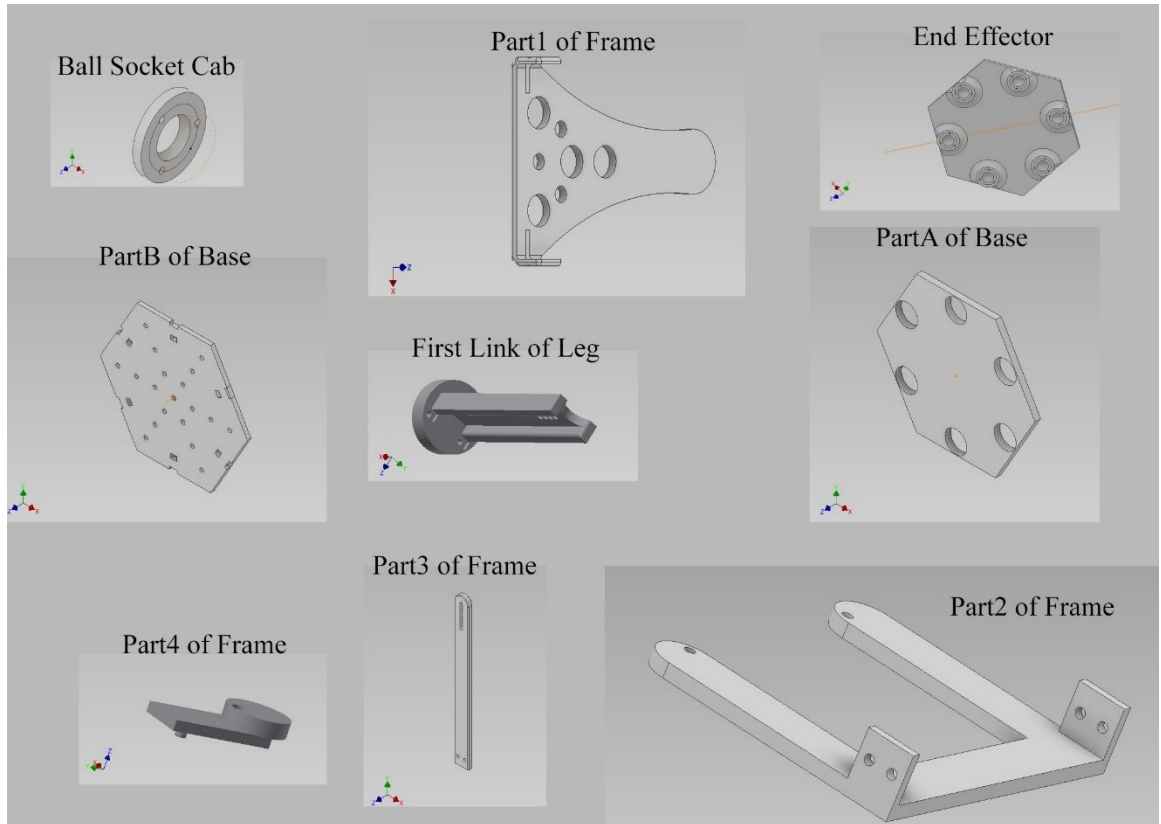


Figure 5. 2 CAD Designs of Parts

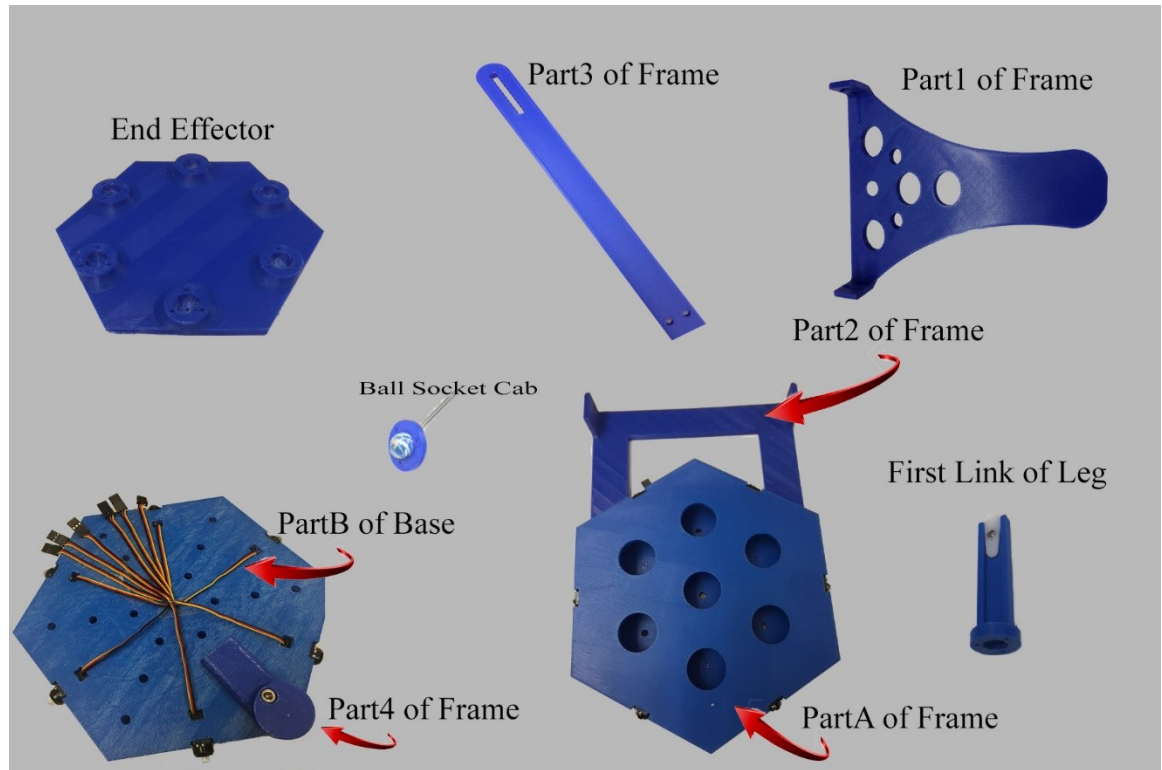


Figure 5.3 3D Printed Mechanical Parts

## 5.2 Electronic Components

Electronic components include HS-5065MG high torque servo motors, a microcontroller (Arduino UNO), Adafruit motor shield as well as a Rayovac AC adaptor for power supply, a breadboard and jumper wires as shown in Fig 5.4.

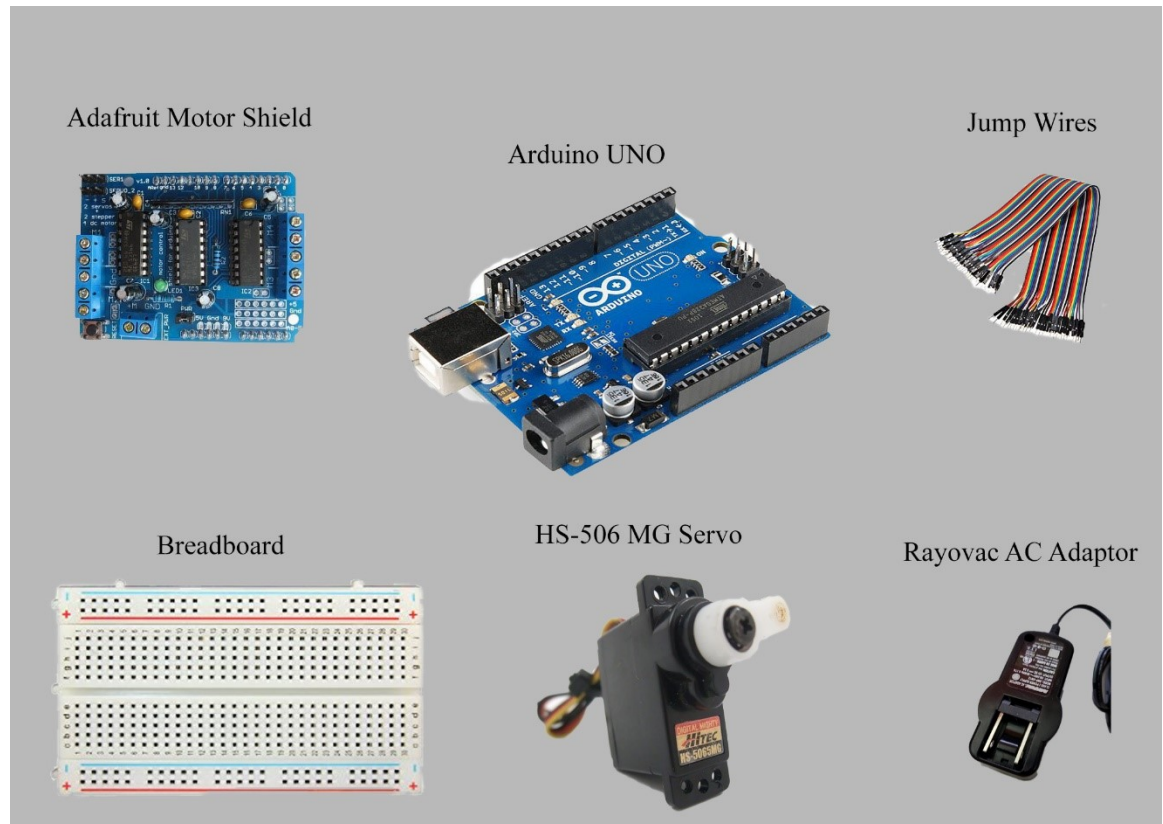


Figure 5. 4 Electronic Components

We chose the servomotor as an actuator for several reasons. First of all, a servomotor allows for precise control of position, velocity and acceleration [28], because it has integrated closed-loop feedback control. Secondly, this servo has high torque and high speed (2.2 kg.cm of torque and a fast transit time of 0.11 second at 6 volts). Since the whole robot, legs and the end effector, is very light (about 20g), the inertia the robot created can be negligible compared to the high torque of the robot. Finally, the size of the servo is small (23.6x11.6x24mm), which fits our design objective.



### 5.3 The Prototype of the Robot

The prototype of the robot is assembled as its CAD model and with its electronic components mounted. Its size, and appearance is illustrated in Fig. 5.5 from various views.

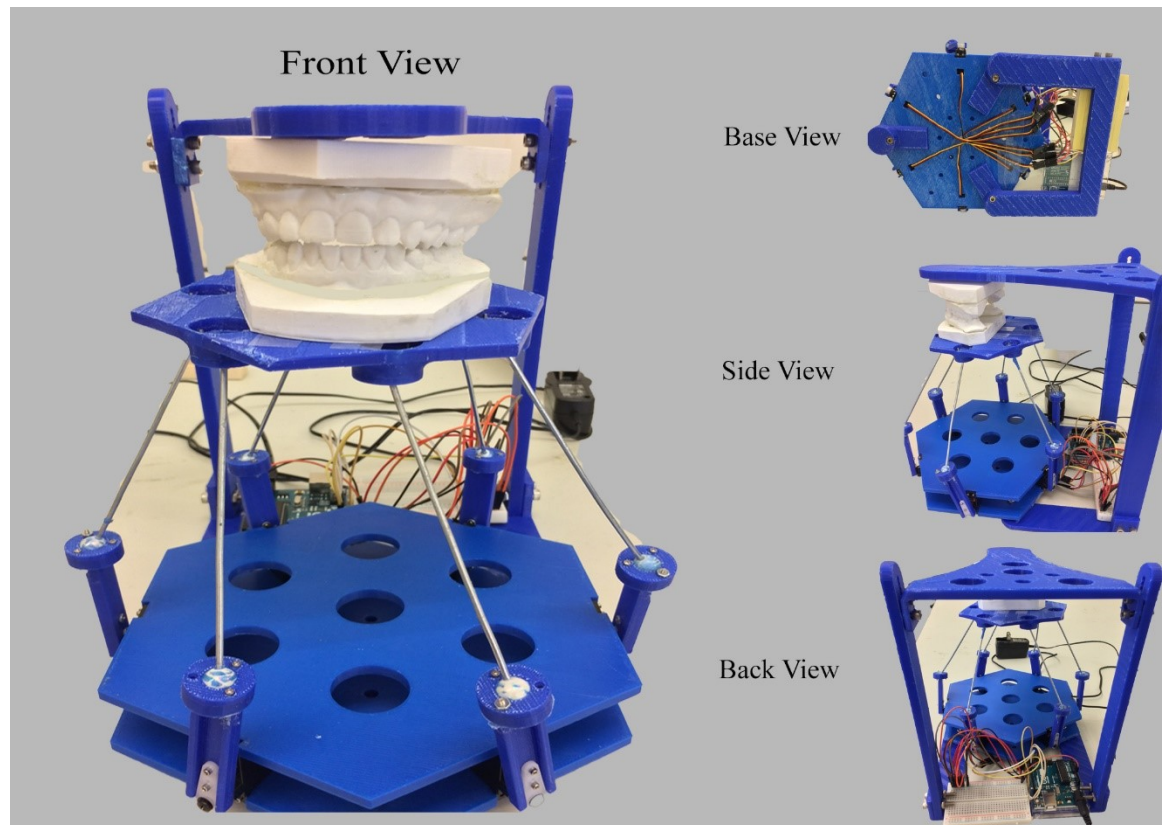


Figure 5. 5 The Prototype of the Robot

The comparison of the robot (270mm x174mm x275mm) with a Denar semi-adjustable articulator (153mm x150mm x140mm), one of the most popular articulators in dentistry, is illustrated in Fig. 5.6

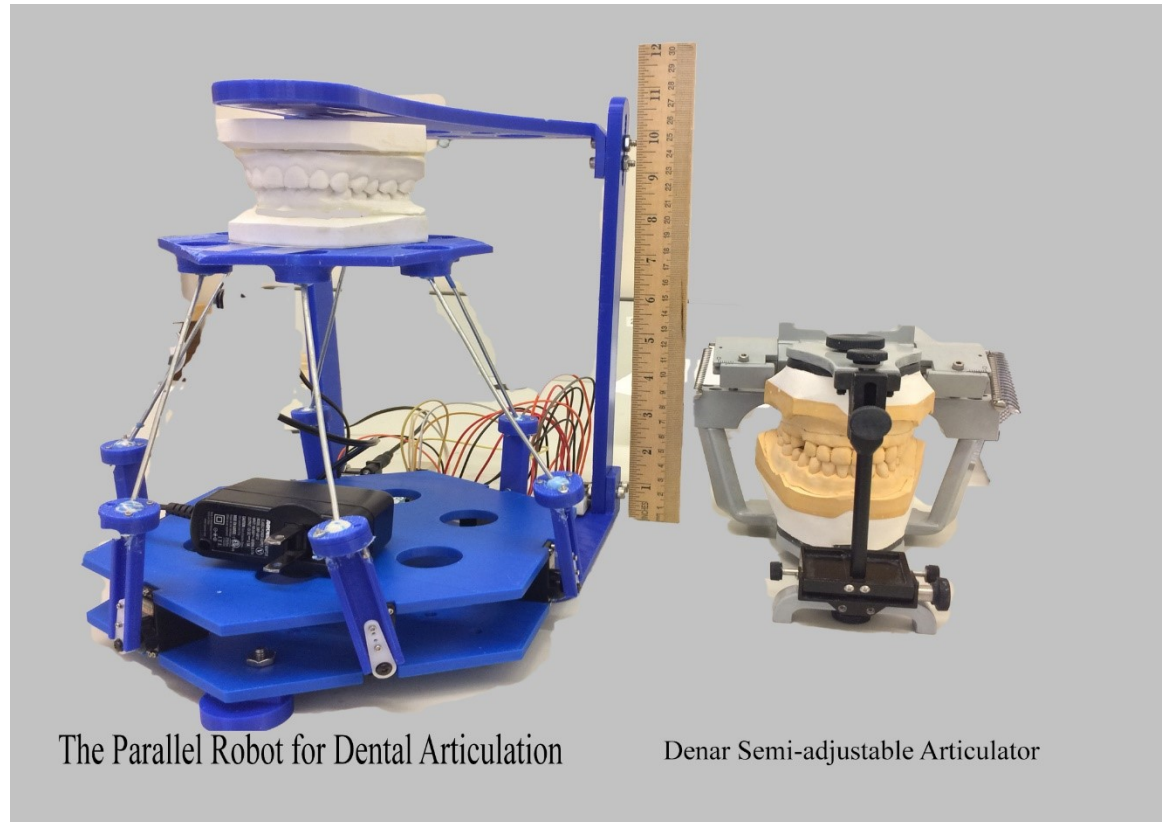


Figure 5. 6 Comparison of the Robot and Denar Articulator

## 5.4 Manufacturing and Prototype Testing

Based on the optimized designs and physical and electronic parts in the previous chapters, the robot is assembled for the testing purpose in this chapter. Since cameras for robot localization are not available, we are not able to validate the accuracy of the motion or position; with the known manufacturing errors of the prototype, its main purpose is to prove out the concept. In this project, the kinematics within the typical range of motion (opening mouth movement) is tested based on inverse kinematics we derived.

Assembling the prototype with dimensions as optimized revealed that one of the assumptions of the optimization needs improvement. The link lengths were minimized based on reaching a given vertical travel distance, under constraints of spherical joint range of motion. It was assumed that all the vertical travel from rotation of  $l_1$  produced vertical translation of  $l_2$ ; however, because of the size mismatch between the fixed and moving platforms, some of length of  $l_2$  is devoted to spanning the horizontal distance between the respective attachment points. Therefore, the lengths  $l_2$  should have a scaling factor greater than 1 applied in order to maintain the optimal workspace characteristics.

To compensate for this in the prototype, a smaller fixed platform was fabricated to allow greater range of motion as in Fig. 5.7 with the size 270mm x 174mm x 275mm, which is closer to the Denar articulator mentioned above. The tradeoff of this is that having fixed and moving platforms of similar size causes the kinematic solution to be poorly conditioned, such that the robot motion is not accurate. In the long run, the solution is to retain the different sizes of fixed and moving platform but built longer links  $l_2$ .

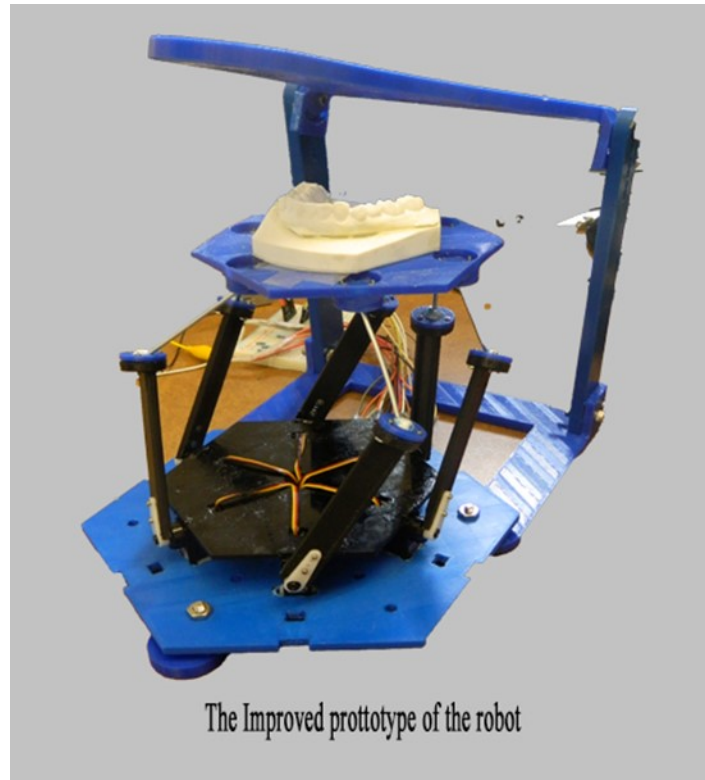


Figure 5. 7 The Improved Robot

A simple open-close motion of the mouth is tested on the robot. The mouth opening of 30 mm and with a  $20^\circ$  angle as illustrated in Fig 5.8 is given to derive the rotational angles in respect to every servo. So, repeating of the motion is coded and the robot acts qualitatively as expected as shown in Fig 5.9.

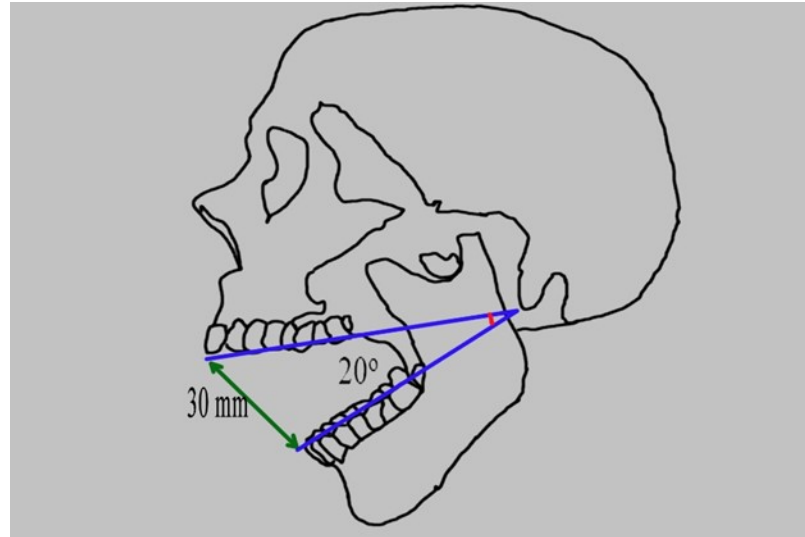


Figure 5. 8The Open-Close Motion

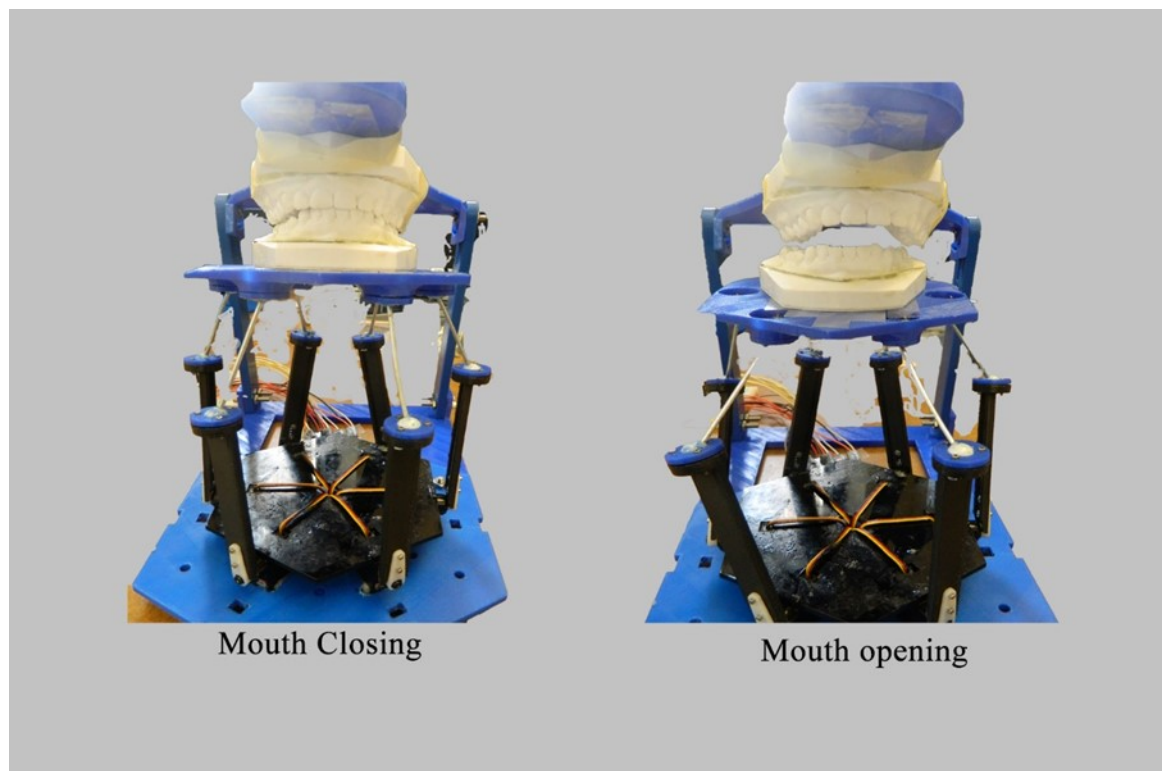


Figure 5. 9 The Test of The Motion

As a result, the servos move accurately with the input angles through command from the Arduino, which is the essential part of the prototype since the kinematics is correct and the optimization has improved the design. However, manufacturing still needs to be improved and the validation of accuracy would be next step with an improved prototype.

## **Chapter 6: Conclusions and Future Work**

### **6.1 Conclusions**

This thesis presents the design, kinematics, optimization and the prototype of the parallel robot for dental articulation. The preliminary design of the robot integrated with its electronic components is tested its movements within its workspace by implementing basic Arduino code successfully.

The objective of this project is to introduce a parallel robot into dental practice. Since the traditional articulator is inherently limited when producing patient-specific dental molds, it is necessary and doable to make an articulator with current technology, which can reduce the trial-error approach to fitting dental work. The dental robot we designed for dental articulation not only addresses the traditional problem in dentistry, but also takes into consideration the technical difficulty of duplicating the positions and motions of an individual patient's jaw in dental clinic. Thus, this is expected to reduce the dentist's chairside time and improve the efficacy of dental workflow. Most importantly, it introduces the new dimension of dynamic motion to the study of dental anatomy, pathology, and dental methods for education and treatment purposes and is a step towards enabling dentists to record and compare the pre- and post-intervention mandible movements as well as analyze static and dynamic occlusions through certain periods of time.

### **6.2 Future Work:**

Future work of the project includes integrating the tracking system which tracks and records the patient's jaw position and movements with the parallel robot after validating computer codes which run the robot. Then, clinical testing will be performed to validate it

through dental practice. Once the validation is done, we will upgrade it with pressure sensors on the end effector and/or the legs. Calculating and analyzing the data collected through the sensors, the dentist is enabled to map out biting forces for every single position of occlusal surfaces and cusps. This will be another significant improvement in dentistry since it is recorded naturally. If it is successfully applied as expected, it has more advantages than the current device, T-Scan, which maps out biting forces by biting a pad.



## References

- [1] Stracke, Edgar, A Critical History of Articulators Based on Geometric Theories of Mandibular Movement: Part 1 Journal of Prosthodontics, 11 (2) June 2002: pp. 135–136.
- [2] Ashish R Jain, Articulators through the Years Revisited: From 1700-1900 – Part I: World J Dent. 2015: 6(4): p.222-225.
- [3] Devendra Chopra, Amrit Tardan et al. The history of articulators: Journal of Dental Sciences & Oral Rehabilitation, Bareilly, April-June 2012: p.27-32.
- [4] Kazem Alemzadeh and Daniel Raabe, Prototyping artificial jaws for the Bristol Dento-Munch Robo-Simulator. in 29th IEEE Annual International Conference of EMBS, New York, February 2007: p. 1453-1456.
- [5] Massimo Callegari and Paolo Marzetti, Proposal of a mechatronic system for reading and analysis of jaw movements and denture testing, Healthcare, medical robots and rehabilitation, 2004: p. 165-171.
- [6] Hideaki Takanobu, Atsuo Takanishi, Kayoko Ohtsuki, and Masatoshi Ohinishi, Mouth opening and closing training with 6-DOF parallel robot, In: Proceedings of the IEEE International Conference on Robotics & Automation, San Francisco, CA, April 2000: p. 1384–1389.
- [7] Waseda University, Dental Robotics Group, June 4th, 2017  
<http://www.takanishi.mech.waseda.ac.jp/top/research/jaws/index.htm>
- [8] Hideaki Takanobu, Atsuo Takanishi, Daisaku Ozawa, Kayoko Ohtsuki, Masatoshi Ohnishi, and Akihisia Okino, Integrated dental robot system for mouth opening and

- closing training, In: Proceedings of the IEEE International Conference on Robotics & Automation, Washington, DC., May 2002: p. 1428-1433.
- [9] Atsuo Takanishi, Hideaki Takabobu, Dental robotics and human model, In: Proceeding of the First International IEEE EMBS Conference on Neural Engineering, Capri Island, Italy. March 2003: p. 20-22.
- [10] Hideaki Takanobu, Takeyuki Yajima, Masayuki Nakazawa, Atsuo Takanishi, Kayoko Ohtsuki, Masatoshi Ohnishi, Quantification of masticatory efficiency with a mastication robot, In: Proceeding of the IEEE International Conference on Robotics & Automation, Leuven, Belgium. May 1998: p. 1635–1640.
- [11] Charles H. Gibbs and Harry C. Lundeen, Jaw movements and forces during chewing and swallowing and their clinical significance, *Advances in Occlusion*, John Wright, November 1981: p. 2-32.
- [12] Koji Hyodo, Development of the joint simulators applying Ni-Ti shape memory alloy, *Seikeigeka Biomechanics*, vol. 7, 1985: p. 231-236.
- [13] WeiLiang Xu, John E. Bronlund and Jules Kieser, A robotic model of human masticatory system for reproducing chewing behaviours, *IEEE Robotics & Automation Magazine*, volume 12, Issue: 2, June 2005: p. 90-98.
- [14] WeiLiang Xu and John E. Bronlund, *Mastication Robots*, Berlin: Springer, Heidelberg, 2010.
- [15] Jeffrey P. Okeson, 2008. *Temporomandibular disorders and occlusion*, 7th edition, Elsevier, pp. 93-108.
- [16] Kawai Y, Murakami H, Shariati B, et al: Do traditional

techniques produce better conventional complete dentures than simplified techniques? *J Dent* 33: 659–668, 2005.

[17] Klineberg I, Kingston D, Murray G: The bases for using a particular occlusal design in tooth and implant-borne reconstructions and complete dentures, *Clin Oral Implants Res* 18(Suppl 3):151–167, 2007.

[18] R.P. Luthra, Renu Gupta, Naresh Kumar, Savisha Mehta, Reena Sirohi: Virtual articulator in prosthetic dentistry: A review. *J Adv Med Dent Scie Res* 2015;3(4):117-121

[19] Padmaja BI, Madan, B, Himabindu G, Manasa C. Virtual articulators in dentistry: a review. *Int J Med Appl Sci.* 2015;4(2):109-14.

[20] Shadakshari S, Nandeeshwar DB, Saritha MK. Virtual articulators: a future oriented technology. *Asian J Med Cli Sci* 2012;1(2):98-101.

[21] Kordass B, Gärtner C, Söhnel A, Bisler A, Voss G, Bockholt U, et al. The virtual articulator in dentistry: concept and development. *Dent Clin North Am.* 2002;46:493-506.

[22] Gärtner C, Kordass B. The virtual articulator: development and evaluation. *Int J Comput Dent.* 2003;6:11-24.

[23] Bisler A, Bockholt U, Kordass B, Suchan , Voss G. The virtual articulator. *Int J Comput Dent.* 2002;5:101-6.

[24] Fang JJ, Kuo TH. Mode ling of mandibular movement. *Comput Biol Med.* 2008;38:1152-62.

- [25] Ortorp, A., Jemt, T., Back, T., Jalevik, T., 2003, Comparisons of precision of fit between cast and CNC-milled titanium implant frameworks for the edentulous mandible, *Int J Prosthodont*, 16(2): 194-200.
- [26] Xiang, R., et al. Trajectory measurement of human mandible and movement test of a chewing robot. *IEEE Conference on Robotics and Biomimetics*, Zhuhai, China, December 6-9, 2015.
- [27] H.D. Taghirad, *Parallel Robots: Mechanics and Control*, CRC Press, NW, ISBN 978-1466555761, 2013.
- [28] <https://web.archive.org/web/20120907042509/http://www.princeton.edu/~mae412/TEXT/NTRAK2002/292-302.pdf>, June 24, 2018
- [29] Stewart D., “A Platform with six degrees of freedom”. *The Inst. of Mech. Engineers*, 1965, vol 180, Pt 1, No 15, pp 371 – 386

## Appendix

### Appendix A

#### Matlab codes for optimization

##### A-1 Creating 6D hypercube vectors within the workspace

```
clear all;clc;

%%
% [x,y,z,c,d,e]=ndgrid(-15:5:15,-2:4:12,60:5:120,-31*pi/180:.2:0,...
% -11*pi/180:.15:11*pi/180,-17*pi/180:.3:17*pi/180)% first iteration
%
% [x,y,z,c,d,e]=ndgrid(-15:5:15,-2:4:12,80:6:140,-31*pi/180:.2:0,...
% -11*pi/180:.15:11*pi/180,-17*pi/180:.3:17*pi/180)% 2nd iteration
%
% [x,y,z,c,d,e]=ndgrid(-15:5:15,-2:4:12,100:6:160,-31*pi/180:.2:0,...
% -11*pi/180:.15:11*pi/180,-17*pi/180:.3:17*pi/180)% 3rd iteration
%
% [x,y,z,c,d,e]=ndgrid(-15:5:15,-2:4:12,118:6:178,-31*pi/180:.2:0,...
% -11*pi/180:.15:11*pi/180,-17*pi/180:.3:17*pi/180)% 4th iteration
%
% [x,y,z,c,d,e]=ndgrid(-15:5:15,-2:4:12,110:5:170,-31*pi/180:.2:0,...
% -11*pi/180:.15:11*pi/180,-17*pi/180:.3:17*pi/180)% 5th iteration
%
% [x,y,z,c,d,e]=ndgrid(-15:5:15,-2:4:12,120:5:180,-31*pi/180:.2:0,...
% -11*pi/180:.15:11*pi/180,-17*pi/180:.3:17*pi/180)% 6th iteration
%
% [x,y,z,c,d,e]=ndgrid(-15:5:15,-2:4:12,120:5:180,-31*pi/180:.2:0,...
% -11*pi/180:.15:11*pi/180,-17*pi/180:.3:17*pi/180)% 7th iteration

% [x,y,z,c,d,e]=ndgrid(-15:5:15,-2:4:12,120:5:180,-31*pi/180:.2:0,...
% -11*pi/180:.15:11*pi/180,-17*pi/180:.3:17*pi/180)% 8th iteration
```

##### A-2 Calculating P, Q, S, H, h1, and h2 values corresponding to the vectors we derived for each leg.

```
syms a b theta r1 r2 z0 z1 z2 l1 l2
z0=0;z1=0;z2=0;
r1=84;r2=47;

% % Initial iteration
% l1=60;l2=60;
% a=5*pi/3; b=5*pi/3; % leg1
% a=0; b=0; % leg2
% a=pi/3; b=pi/3; % leg3
% a=2*pi/3; b=2*pi/3; %leg4
% a=pi; b=pi; %leg5
% a=4*pi/3; b=4*pi/3; %leg6
%% 2nd iteration
```

```

% a=5*pi/3; b=5*pi/3; l1=62.5 ;l2=80; % leg1
% a=0; b=0; l1=60.4;l2=70; % leg2
% a=pi/3; b=pi/3; l1=58;l2=70;% leg3
% a=2*pi/3; b=2*pi/3;l1=58;l2=70; %leg4
% a=pi; b=pi; l1=60.4;l2=70;%leg5
% a=4*pi/3; b=4*pi/3;l1=62.5;l2=80; %leg6

%% 3rd iteration
% l1 = 63 60.5 68.5;
% l2= 98 87 79;
% a=5*pi/3; b=5*pi/3; l1=63 ;l2=98; % leg1
% a=0; b=0; l1=60.5;l2=87; % leg2
% a=pi/3; b=pi/3; l1=68.5; l2=79;% leg3
% a=2*pi/3; b=2*pi/3;l1=66; l2=68; %leg4
% a=pi; b=pi; l1=60.5;l2=87; %leg5
% a=4*pi/3; b=4*pi/3; l1=63 ;l2=98; %leg6
%% 4th iteration
% l1 = 63.6 60.5 64;
% l2= 116 105 93;
% a=5*pi/3; b=5*pi/3; l1=63.6 ;l2=116; % leg1
% a=0; b=0; l1=60.5;l2=105; % leg2
% a=pi/3; b=pi/3; l1=64; l2=93;% leg3
% a=2*pi/3; b=2*pi/3;l1=64; l2=93; %leg4
% a=pi; b=pi; l1=60.5;l2=105; %leg5
% a=4*pi/3; b=4*pi/3;l1=63.6 ;l2=116;%leg6
%% 5th iteration
% l1 = 64.2 60.7 60.4;
% l2= 108 92 86.7;
% a=5*pi/3; b=5*pi/3; l1=64.2 ;l2=108; % leg1
% a=0; b=0; l1=60.7;l2=92; % leg2
% a=pi/3; b=pi/3; l1=60.4; l2=86.7;% leg3
% a=2*pi/3; b=2*pi/3; l1=60.4; l2=86.7; %leg4
% a=pi; b=pi;l1=60.7;l2=92; %leg5
% a=4*pi/3; b=4*pi/3; l1=64.2 ;l2=108; %leg6
%% 6th iteration
% l1 = 64.2 60.6 60.2;
% l2= 126 112 101.6;
% a=5*pi/3; b=5*pi/3; l1=64.2 ;l2=126; % leg1
% a=0; b=0; l1=60.6;l2=112; % leg2
% a=pi/3; b=pi/3; l1=60.2; l2=101.6;% leg3
% a=2*pi/3; b=2*pi/3; l1=60.2; l2=101.6; %leg4
% a=pi; b=pi;l1=60.6;l2=112; %leg5
% a=4*pi/3; b=4*pi/3;l1=64.2 ;l2=126; %leg6
%% 7th iteration
% l1 = 64.1 60.5 60.3;
% l2= 130.7 117 106.2;
% a=5*pi/3; b=5*pi/3; l1=64.1 ;l2=130.7; % leg1
% a=0; b=0; l1=60.5;l2=117; % leg2
% a=pi/3; b=pi/3; l1=60.3; l2=106.2;% leg3
% a=2*pi/3; b=2*pi/3; l1=60.3; l2=106.2; %leg4
% a=pi; b=pi;l1=60.5;l2=117; %leg5
% a=4*pi/3; b=4*pi/3; l1=64.1 ;l2=130.7; %leg6
%% 8th iteration
% l1 = 64.1 60.4 60.2;
% l2= 128.8 117 103.7;

```

```

% a=5*pi/3; b=5*pi/3; l1=64.1 ;l2=128.8 ; % leg1
% a=0; b=0; l1=60.4;l2=117; % leg2
% a=pi/3; b=pi/3; l1=60.2; l2=103.7;% leg3
% a=2*pi/3; b=2*pi/3; l1=60.2; l2=103.7; %leg4
% a=pi; b=pi;l1=60.5;l2=117; %leg5
% a=4*pi/3; b=4*pi/3; l1=64.1 ;l2=128.8; %leg6
%%
% R=[cos(d)*cos(e) -sin(e) sin(d)*cos(e); cos(c)*cos(d)*sin(e)+...
% sin(c)*sin(d) cos(c)*cos(e) cos(c)*sin(d)*sin(e)-sin(c)*cos(d);...
% sin(c)*cos(d)*sin(e)-cos(c)*sin(d) sin(c)*cos(e) ...
% sin(c)*sin(d)*sin(e)+cos(c)*cos(d)];
% Cd=[r2*cos(b); r2*sin(b);z2];
% Do=[x;y;z];
% Co=Do+R*Cd;
% Bo=[l1*sin(a)*sin(theta)+r1*cos(a); -
l1*cos(a)*sin(theta)+r1*sin(a);...
% l1*cos(theta)+z1];

P=x - r2*sin(b).*sin(e) + z2*sin(d).*cos(e) +
r2*cos(b).*cos(d).*cos(e);
Q=y - z2*(cos(d).*sin(c) - cos(c).*sin(d).*sin(e)) + ...
r2*cos(b).(sin(c).*sin(d) + cos(c).*cos(d).*sin(e)) +...
r2*cos(c).*cos(e).*sin(b);
S= z + z2*(cos(c).*cos(d) + sin(c).*sin(d).*sin(e)) - ...
r2*cos(b).(cos(c).*sin(d) - cos(d).*sin(c).*sin(e)) + ...
r2*cos(e).*sin(b).*sin(c);
H=P.^2+Q.^2+S.^2+z01^2+r1^2+l1^2-l2^2-2*P.*r1*cos(a)- ...
2*Q.*r1*sin(a)-2*S.*z01;
h1=l1*Q.*cos(a)-l1*P.*sin(a);
h2=l1*(z01+S);

```

### A-3 The code for deriving theta values of each leg

```

for i1=1:size(H,1)
    for i2=1:size(H,2)
        for i3=1:size(H,3)
            for i4=1:size(H,4)
                for i5=1:size(H,5)
                    for i6=1:size(H,6)
                        h1temp = h1(i1,i2,i3,i4,i5,i6);
                        h2temp = h2(i1,i2,i3,i4,i5,i6);
                        Htemp = H(i1,i2,i3,i4,i5,i6);
                        xtemp=x(i1,i2,i3,i4,i5,i6) ;
                        ytemp = y(i1,i2,i3,i4,i5,i6) ;
                        ztemp=z(i1,i2,i3,i4,i5,i6);
                        ctemp=c(i1,i2,i3,i4,i5,i6) ;
                        dtemp=d(i1,i2,i3,i4,i5,i6) ;
                        etemp=e(i1,i2,i3,i4,i5,i6) ;
                        P=xtemp - r2*sin(b).*sin(etestemp) + z2*sin(dtemp).*cos(etestemp) +
r2*cos(b).*cos(dtemp).*cos(etestemp);
                        Q=ytemp - z2*(cos(dtemp).*sin(ctemp) -
cos(ctemp).*sin(dtemp).*sin(etestemp)) +
r2*cos(b).(sin(ctemp).*sin(dtemp) +
cos(ctemp).*cos(dtemp).*sin(etestemp)) +
r2*cos(ctemp).*cos(etestemp).*sin(b);

```

```

        S= ztemp + z2*(cos(ctemp).*cos(dtemp) +
sin(ctemp).*sin(dtemp).*sin(etemp)) -
r2*cos(b).*cos(ctemp).*sin(dtemp) -
cos(dtemp).*sin(ctemp).*sin(etemp)) +
r2*cos(etemp).*sin(b).*sin(ctemp);
        AC=((P-r1*cos(a))^2+(Q-r1*sin(a))^2+(S-z1)^2)^(1/2);
        if AC>180 && AC<90
            theta(i1,i2,i3,i4,i5,i6) = NAN;
        else

            F = @(thetatemp,h1temp,h2temp,Htemp) 2*h1temp.*sin(thetatemp)-
            2*h2temp.*cos(thetatemp)+Htemp;
            thetatemp=pi/4;
            theta6(i1,i2,i3,i4,i5,i6)=fzero(@(thetatemp)
            F(thetatemp,h1temp,h2temp,Htemp),0);
            end
            end
            end
            end
            end
            end
            end
end
end

```

#### A-4 code for finding the vector AC's value and maximum and minimum values of AC for each leg.

```

syms a b r1 r2 z0 z01 z1 z2 l1 l2
z0=0;z01=0;z1=0;z2=0;
r1=84;r2=47;

%% initial iteration
% l1=60;l2=60;
% a=5*pi/3; b=279.21*pi/180; % leg1
% a=0; b=20.79*pi/180; % leg2
% a=pi/3; b=39.21*pi/180; % leg3
% a=2*pi/3; b=140.69*pi/180; %leg4
% a=pi; b=159.21*pi/180; %leg5
% a=4*pi/3; b=260.79*pi/180; %leg6
%% 2nd iteration

% a=5*pi/3; b=5*pi/3; l1=62.5 ;l2=80; % leg1
% a=0; b=0; l1=60.4;l2=70; % leg2
% a=pi/3; b=pi/3; l1=58;l2=70;% leg3
% a=2*pi/3; b=2*pi/3;l1=58;l2=70; %leg4
% a=pi; b=pi; l1=60.4;l2=70;%leg5
% a=4*pi/3; b=4*pi/3;l1=62.5;l2=80; %leg6

%% 3rd iteration
% l1 = 63 60.5 68.5;
% l2= 98 87 79;
% a=5*pi/3; b=5*pi/3; l1=63 ;l2=98; % leg1
% a=0; b=0; l1=60.5;l2=87; % leg2

```



```

% a=pi/3; b=pi/3; l1=68.5; l2=79;% leg3
% a=2*pi/3; b=2*pi/3;l1=66; l2=68; %leg4
% a=pi; b=pi; l1=67;l2=80; %leg5
% a=4*pi/3; b=4*pi/3;l1=69 ;l2=81; %leg6
%% 4th iteration
% l1 = 63.6 60.5 64;
% l2= 116 105 93;
% a=5*pi/3; b=5*pi/3; l1=63.6 ;l2=116; % leg1
% a=0; b=0; l1=60.5;l2=105; % leg2
% a=pi/3; b=pi/3; l1=64; l2=93;% leg3
% a=2*pi/3; b=2*pi/3;l1=64; l2=93; %leg4
% a=pi; b=pi; l1=60.5;l2=105; %leg5
% a=4*pi/3; b=4*pi/3;l1=63.6 ;l2=116;%leg6
%% 5th iteration
% l1 = 64.2 60.7 60.4;
% l2= 108 92 86.7;
% a=5*pi/3; b=5*pi/3; l1=64.2 ;l2=108; % leg1
% a=0; b=0; l1=60.7;l2=92; % leg2
% a=pi/3; b=pi/3; l1=60.4; l2=86.7;% leg3
% a=2*pi/3; b=2*pi/3; l1=60.4; l2=86.7; %leg4
% a=pi; b=pi;l1=60.7;l2=92; %leg5
% a=4*pi/3; b=4*pi/3; l1=64.2 ;l2=108; %leg6
%% 6th iteration
% l1 = 64.2 60.6 60.2;
% l2= 126 112 101.6;
% a=5*pi/3; b=5*pi/3; l1=64.2 ;l2=126; % leg1
% a=0; b=0; l1=60.6;l2=112; % leg2
% a=pi/3; b=pi/3; l1=60.2; l2=101.6;% leg3
% a=2*pi/3; b=2*pi/3; l1=60.2; l2=101.6; %leg4
% a=pi; b=pi;l1=60.6;l2=112; %leg5
% a=4*pi/3; b=4*pi/3;l1=64.2 ;l2=126; %leg6
%% 7th iteration
% l1 = 64.1 60.5 60.3;
% l2= 130.7 117 106.2;
% a=5*pi/3; b=5*pi/3; l1=64.1 ;l2=130.7; % leg1
% a=0; b=0; l1=60.5;l2=117; % leg2
% a=pi/3; b=pi/3; l1=60.3; l2=106.2;% leg3
% a=2*pi/3; b=2*pi/3; l1=60.3; l2=106.2; %leg4
% a=pi; b=pi;l1=60.5;l2=117; %leg5
% a=4*pi/3; b=4*pi/3; l1=64.1 ;l2=130.7; %leg6
%% 8th iteration
% l1 = 64.1 60.4 60.2;
% l2= 128.8 117 103.7;
% a=5*pi/3; b=5*pi/3; l1=64.1 ;l2=128.8 ; % leg1
% a=0; b=0; l1=60.4;l2=117; % leg2
% a=pi/3; b=pi/3; l1=60.2; l2=103.7;% leg3
% a=2*pi/3; b=2*pi/3; l1=60.2; l2=103.7; %leg4
% a=pi; b=pi;l1=60.5;l2=117; %leg5
% a=4*pi/3; b=4*pi/3; l1=64.1 ;l2=128.8; %leg6
for i1=1:size(x,1)
    for i2=1:size(x,2)
        for i3=1:size(x,3)
            for i4=1:size(x,4)
                for i5=1:size(x,5)
                    for i6=1:size(x,6)
                        xtemp=x(i1,i2,i3,i4,i5,i6) ;
                        ytemp = y(i1,i2,i3,i4,i5,i6) ;
                    end
                end
            end
        end
    end
end

```

```

ztemp=z(i1,i2,i3,i4,i5,i6);
ctemp=c(i1,i2,i3,i4,i5,i6);
dtemp=d(i1,i2,i3,i4,i5,i6);
etemp=e(i1,i2,i3,i4,i5,i6);
P(i1,i2,i3,i4,i5,i6)=xtemp - r2*sin(b).*sin(etemp) +...
z2*sin(dtemp).*cos(etemp) +
r2*cos(b).*cos(dtemp).*cos(etemp);
Q(i1,i2,i3,i4,i5,i6)=ytemp - z2*(cos(dtemp).*sin(ctemp) - ...
cos(ctemp).*sin(dtemp).*sin(etemp)) +
r2*cos(b).*(sin(ctemp).*...
sin(dtemp) + cos(ctemp).*cos(dtemp).*sin(etemp)) + ...
r2*cos(ctemp).*cos(etemp).*sin(b);
S(i1,i2,i3,i4,i5,i6)= ztemp + z2*(cos(ctemp).*cos(dtemp) +....
sin(ctemp).*sin(dtemp).*sin(etemp)) -
r2*cos(b).*(cos(ctemp).*...
sin(dtemp) - cos(dtemp).*sin(ctemp).*sin(etemp)) + ...
r2*cos(etemp).*sin(b).*sin(ctemp);
Ptemp=P(i1,i2,i3,i4,i5,i6);
Qtemp=Q(i1,i2,i3,i4,i5,i6);
Stemp=S(i1,i2,i3,i4,i5,i6);
AC(i1,i2,i3,i4,i5,i6)=((Ptemp-r1*cos(a))^2+(Qtemp-
r1*sin(a))^2+...
(Stemp-z1)^2)^(1/2);

end
end
end
end
end
end

```

```

ACmx=max( reshape(AC,[i1*i2*i3*i4*i5*i6],1))% the maximumvae of AC
ACmn=min( reshape(AC,[i1*i2*i3*i4*i5*i6],1))% the minimum value of AC

```

#### A-5 Ultimate values for $l_{1i}$ and $l_{2i}$

```

% % 1st
% ACmx = [ 164.3623 140.5773 137.2969];
% ACmn = [72.8352 54.5726 56.9260];
% result of 2nd iteration
% % L1 = 64.7194 60.8145 56.8308;
% % L2 = 99.6429 79.7628 80.4661;
% l1 and l2 values for next iteration
% l1 = 62.5 60.4 58;
% l2= 80 70 70
% % 2nd
% ACmx = [179.7573 164.3276 147.9616];
% ACmn = [88.5726 78.2144 63.9522];
% result of 1st iteration
% L1 = 64.4773 60.8912 59.4036
% L2 = 115.2800 103.4364 88.5580
% l1 and l2 values for next iteration
% l1 = 63 60.5 68.5;
% l2= 98 87 79;

```

```

%% 3rd
% ACmx = [ 198.5127 183.2728 167.0008];
% ACmn = [ 107.5790 97.5499 82.2368];
% result of 1st iteration
% % L1 = 64.2998 60.6152 59.9372;
% % L2 = 134.2129 122.6576 107.0636;
% l1 and l2 values for next iteration
% l1 = 63.6 60.5 64;
% l2= 116 105 93;

%% 4th
% ACmx = [ 215.5839 200.4988 184.3101];
% ACmn = [124.9502 115.1460 99.2603];
% result of 1st iteration
% % L1 = 64.7194 60.8145 56.8308;
% % L2 = 99.6429 79.7628 80.4661;
% l1 and l2 values for next iteration
% l1 = 64.2 60.7 60.4;
% l2= 108 92 86.7;

%% 5st
% ACmx = [ 207.9774 192.8254 176.6000];
% ACmn = [117.2062 107.3090 91.6483];
% result of 1st iteration
% % L1 = 64.1849 60.4692 60.0699;
% % L2 = 143.7925 132.3562 116.5301;
% l1 = 64.2 60.6 60.2;
% l2= 126 112 101.6;

%% 6st
% ACmx = [ 217.4900 202.4211 186.2414];
% ACmn = [ 126.8912 117.1087 101.1727];
% result of 1st iteration
% % L1 = 64.0630 60.3250 60.1527;
% % L2 = 153.4270 142.0961 126.0887;
% l1 and l2 values for next iteration
% l1 = 64.1 60.5 60.3;
% l2= 130.7 117 106.2;

%% 7st
% ACmx = [ 217.4900 202.4211 186.2414];
% ACmn = [ 126.8912 117.1087 101.1727];
% result of 1st iteration
% % L1 = 64.0630 60.3250 60.1527;
% % L2 = 153.4270 142.0961 126.0887;
% l1 and l2 values for next iteration
% l1 = 64.1 60.4 60.2;
% l2= 128.8 117 103.7;

%% 8st
% ACmx = [ 217.4900 202.4211 186.2414];
% ACmn = [ 126.8912 117.1087 101.1727];
% result of 1st iteration
% % L1 = 64.0630 60.3250 60.1527;
% % L2 = 153.4270 142.0961 126.0887;

```

```
% l1 and l2 values for next iteration
% l1 = 64.1 60.4 60.2;
% l2= 128.8 117 103.7;
```

```
L1=(ACmx-ACmn) ./2^(1/2);
L2=ACmx-L1;
```

### A-6 Testing Robot

```
%% to test the robot
clear all;clc;
syms a b theta r1 r2 z0 z01 z1 z2 l1 l2
z0=0;z01=0;z1=0;z2=0;
r1=60 ;r2=47 ;
% l1=60;l2=120;
% a=5*pi/3; b=5*pi/3; l1=90 ;l2=70; % leg1
% a=0; b=0; l1=90 ;l2=60; % leg2
% a=pi/3; b=pi/3; l1=90 ;l2=50;% leg3
% a=2*pi/3; b=2*pi/3; l1=90 ;l2=50; %leg4
% a=pi; b=pi; l1=90;l2=60;%leg5
% a=4*pi/3; b=4*pi/3; l1=90 ;l2=70; %leg6
%% the initial position
% x=0 ;y=0 ;z=130;
% c=0 ; d=0 ;e=0;
%% open mouth1 (estimated)
% x=0 ;y=0 ;z=115;
% c=.3491 ; d=0 ;e=0;
%% open mouth2 (estimated)
% x=0 ;y=0 ;z=100;
% c=.5236 ; d=0 ;e=0;

P =x - r2.*sin(b).*sin(e) + z2.*sin(d).*cos(e) +...
r2.*cos(b).*cos(d).*cos(e);
Q =y - z2.*(cos(d).*sin(c) - cos(c).*sin(d).*sin(e)) +...
r2.*cos(b).*(sin(c).*sin(d) + cos(c).*cos(d).*sin(e)) +...
r2.*cos(c).*cos(e).*sin(b);
S = z + z2.*(cos(c).*cos(d) + sin(c).*sin(d).*sin(e)) -...
r2.*cos(b).*(cos(c).*sin(d) - cos(d).*sin(c).*sin(e)) +...
r2.*cos(e).*sin(b).*sin(c);
AC=((P-r1.*cos(a)).^2+(Q-r1.*sin(a)).^2+(S-z1).^2).^(1/2);
if AC > 140 & AC<90
theta = NAN;
else

H=P.^2+Q.^2+S.^2+z01.^2+r1.^2+l1.^2-l2.^2-2*P.*r1.*cos(a)-...
2*Q.*r1.*sin(a)-2*S.*z01;
h1=l1.*Q.*cos(a)-l1.*P.*sin(a);
h2=l1.*(z01+S);

F = @(theta0,h1,h2,H) 2*h1.*sin(theta0)-2*h2.*cos(theta0)+H;
theta0=pi/4;
```

```
theta=fzero(@(theta0) F(theta0,h1,h2,H),0);
end
```

## Appendix B

### Arduino Codes

#### B-1 Code for finding the revolute range of Servo

```
#include <Servo.h> // Loading the servo library.

int pos=0; // initialize the pos variable

int servoPin=9; // the servo hooked to pin 9

int servoDelay=25;

Servo myBaby;// called my Baby

void setup() {

    Serial.begin(9600);

    myBaby.attach(servoPin);

}

void loop() {

    Serial.println(" the Position"); // prompt user for input

    while (Serial.available()==0){

    }

    pos=Serial.parseInt();// read user input

    myBaby.write(pos); // write pos to servo

}
```

## B-2 Code for the opening-closing movement

```
#include <Servo.h>

// define our servos

Servo servo1;

Servo servo2;

Servo servo3;

Servo servo4;

Servo servo5;

Servo servo6;

// Srvo position in degrees

int servoPos =0;

void setup ()

{

    //Define servo signal input (Digital PWM 1-2-3-4-5-6)

    servo1.attach(3);

    servo2.attach(5);

    servo3.attach(6);

    servo4.attach(9);

    servo5.attach(10);
```

```
servo6.attach(11);

}

void loop()

{

// Scan from 30 to 150 degrees

for(servoPos = 20; servoPos < 80; servoPos += 15)

{

servo1.write(servoPos);

servo6.write(servoPos);

}

for(servoPos = 20; servoPos < 60; servoPos += 10)

{

servo2.write(servoPos);

servo5.write(servoPos);

}

for(servoPos = 20; servoPos < 40; servoPos +=5)

{

servo3.write(servoPos);

servo4.write(servoPos);
```

```
}

// now scan back from 150 to 30 degrees

  for(servoPos = 80; servoPos > 20; servoPos -=15)

  {

    servo1.write(servoPos);

    servo6.write(servoPos);

  }

// now scan back from 150 to 30 degrees

  for(servoPos = 60; servoPos > 20; servoPos -=10)

  {

    servo2.write(servoPos);

    servo5.write(servoPos);

  }

// now scan back from 150 to 30 degrees

  for(servoPos = 40; servoPos > 20; servoPos -=5)

  {

    servo3.write(servoPos);
```

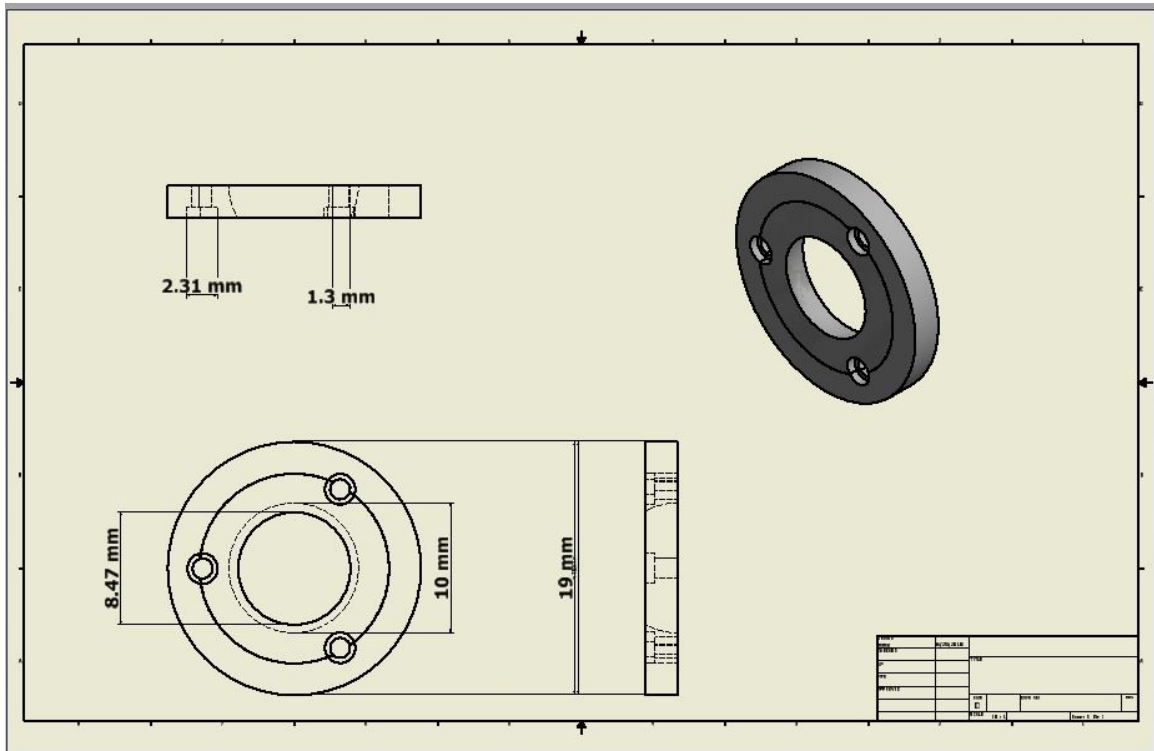


```
servo4.write(servoPos);  
  
}  
  
}
```

### Appendix C

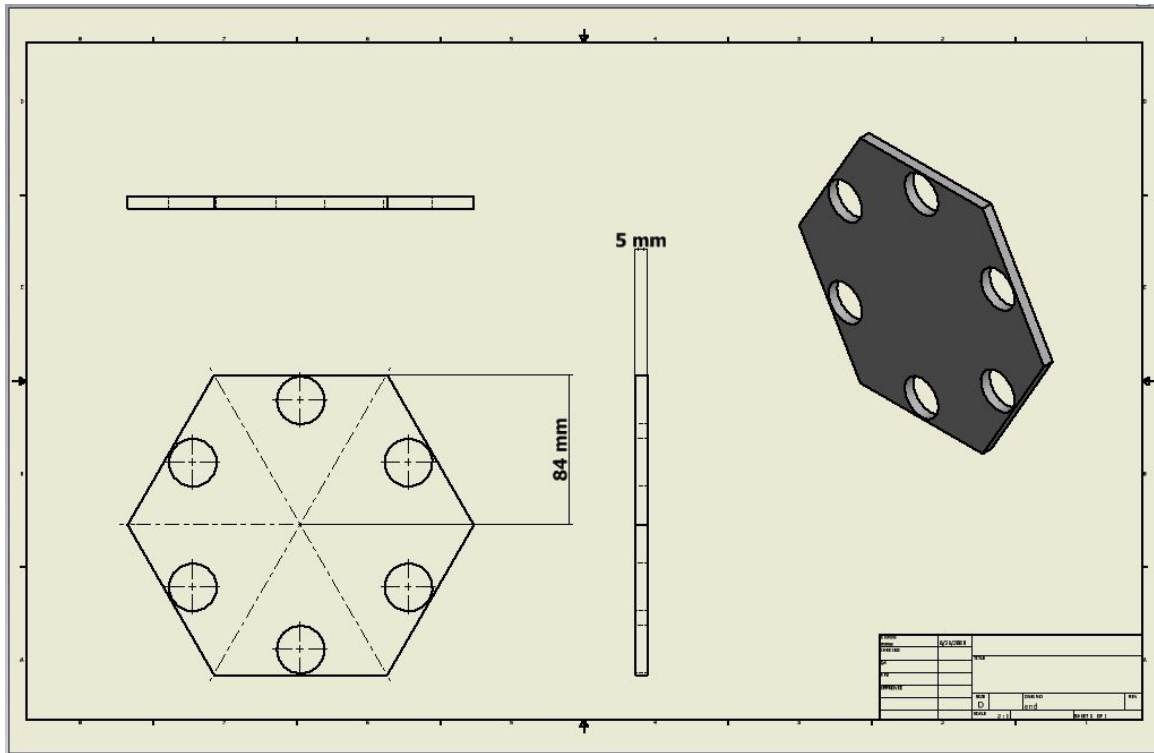
Profiles of parts

C-1 Ball Socket Cab

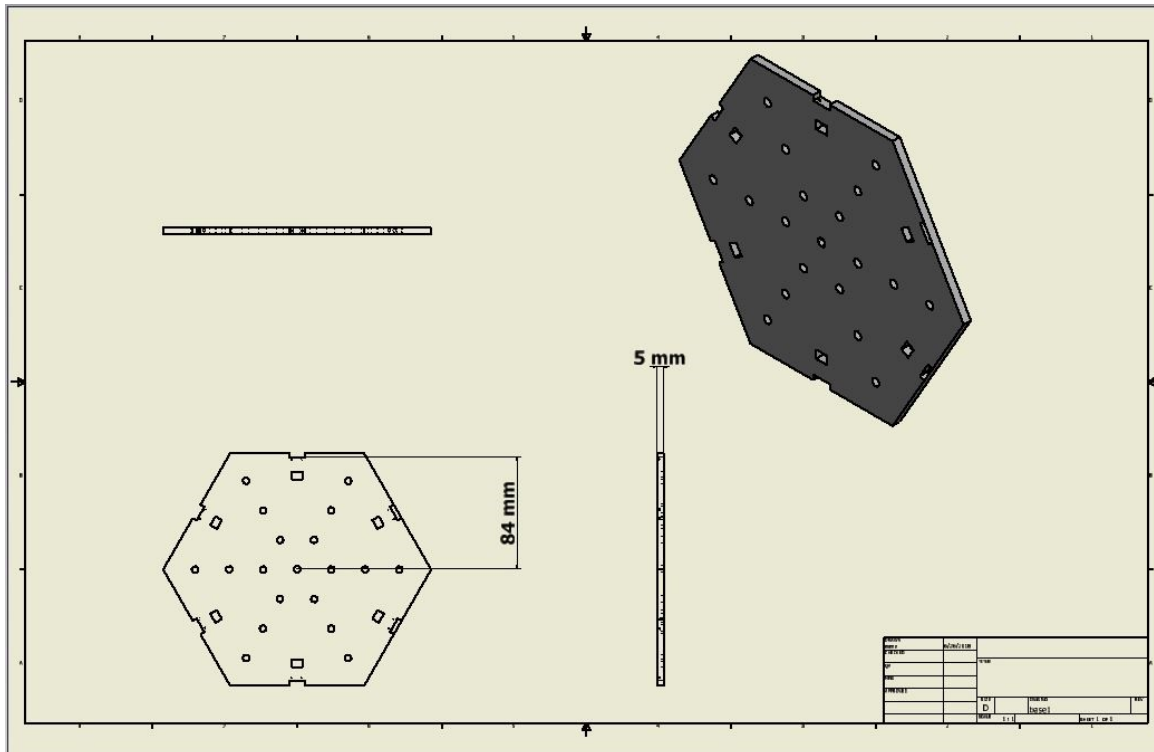




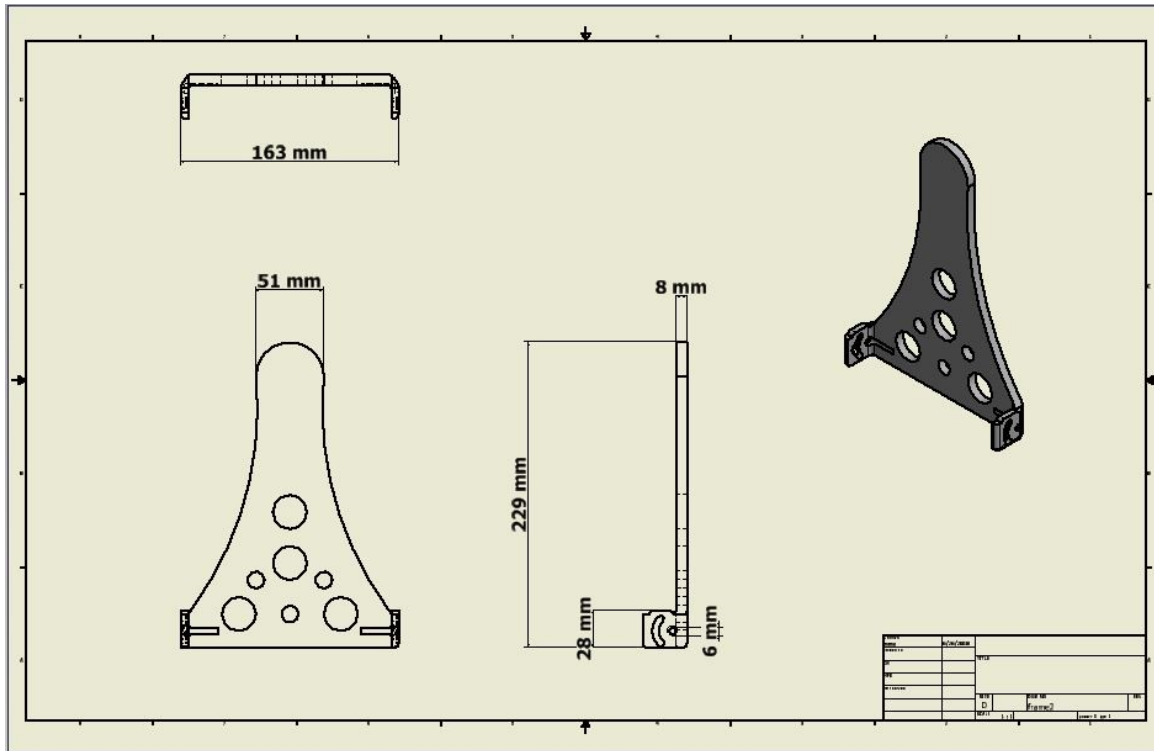
C-4 Part A of Base



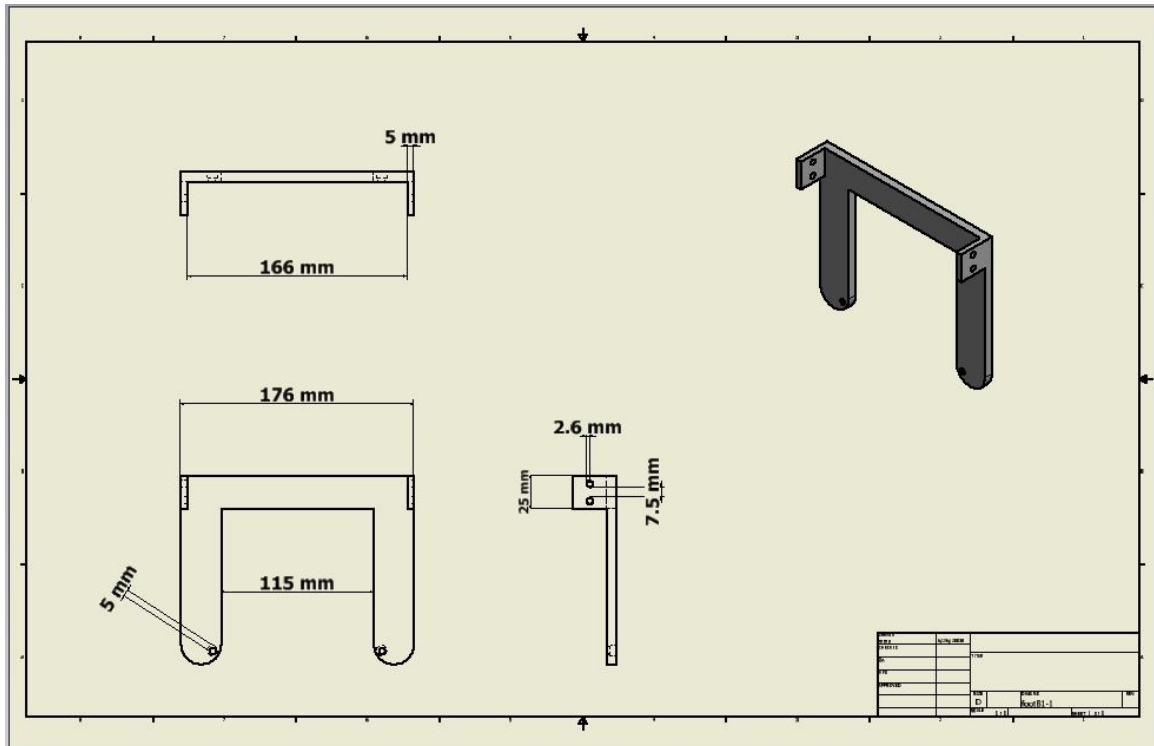
C-5 Part B of Base



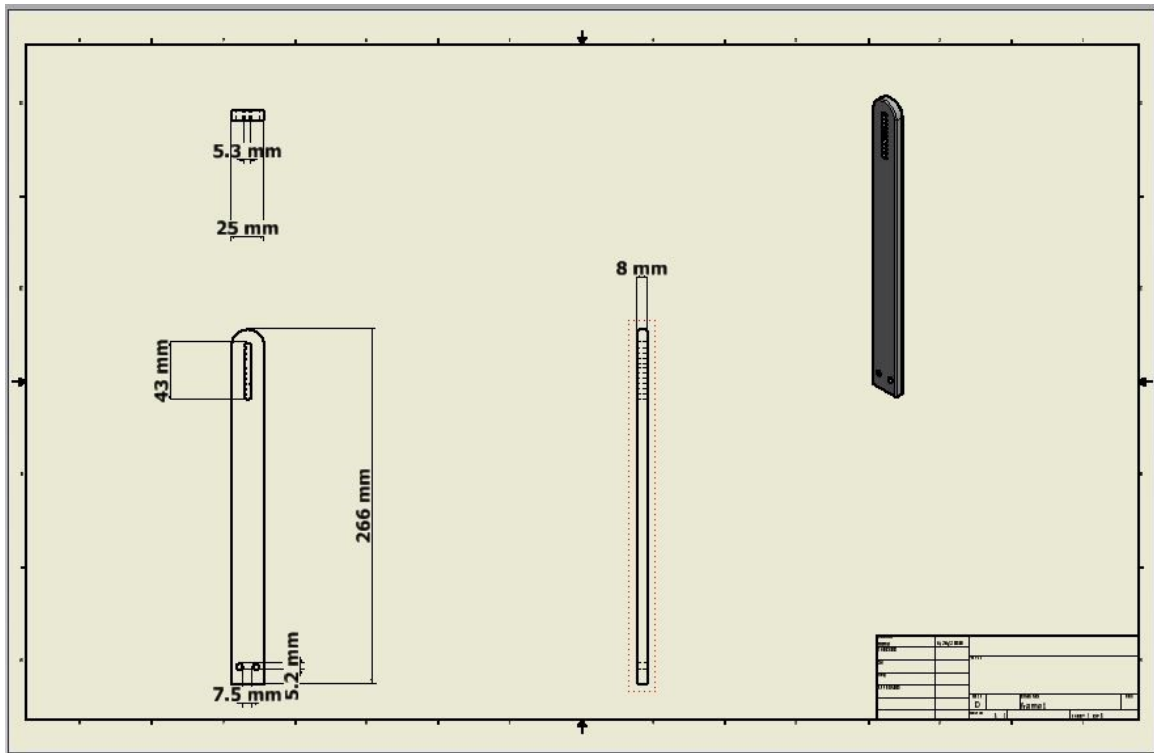
C-6 Part 1 of Frame



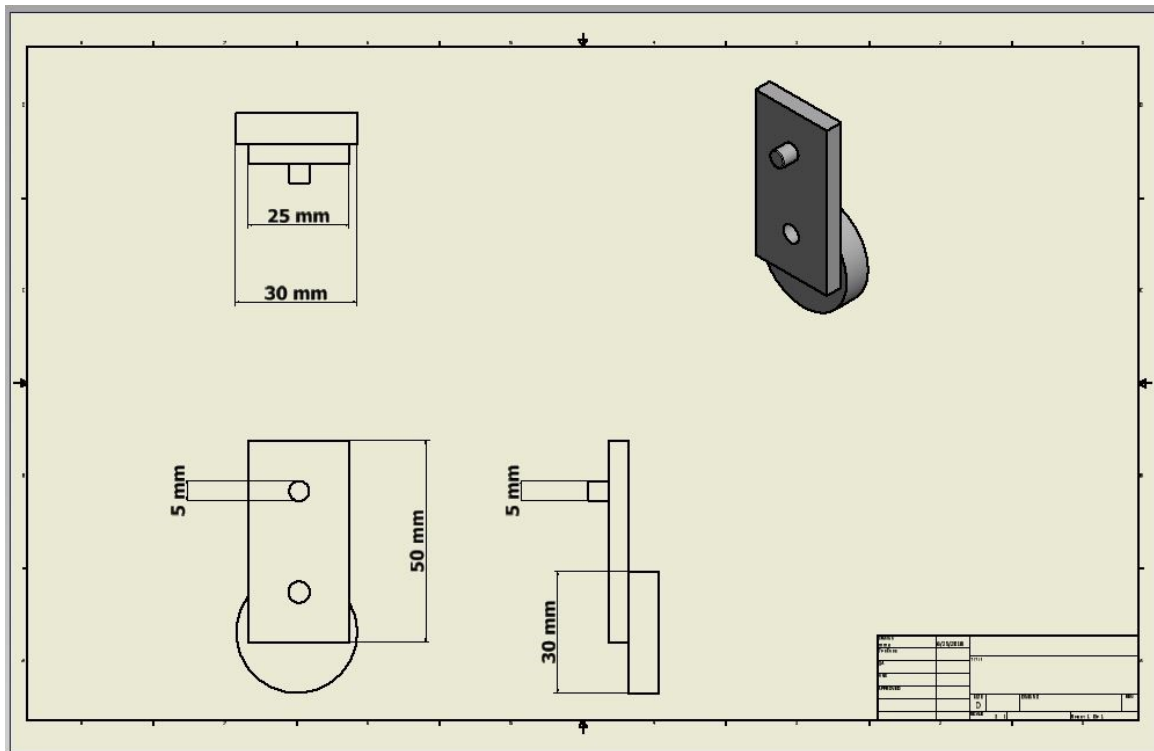
C-7 Part 2 of Frame



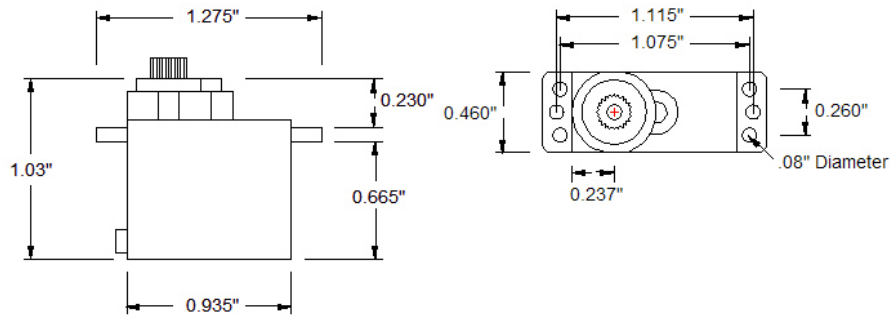
C-8 Part 3 of Frame



C-9 Part 4 of Frame



## C-10 HS - 5065MG Servo

**Programable Features:**

- Dead Band Width
- Direction of Rotation
- Speed of Rotation (slower)
- End Points (up to 120 degrees)
- Neutral Points
- Fail Safe On/Off
- Fail Safe Points
- Resolution (default is set at high)
- Overload Protection (default is off)

Dimensions	0.92" x 0.45" x 0.94" (23.37 x 11.43 x 23.88mm)
Product Weight	0.42oz (11.9g)
Output Shaft Style	25 tooth (B1) spline
Voltage Range	4.8V - 6.0V
No-Load Speed (4.8V)	0.14 sec/60°
No-Load Speed (6.0V)	0.11 sec/60°
Stall Torque (4.8V)	24.99oz/in. (1.8kg.cm)
Stall Torque (6.0V)	30.55oz/in. (2.2kg.cm)
Max PWM Signal Range (Standard)	750-2250µsec
Travel per µs (out of box)	.085°/µsec
Travel per µs (reprogrammed normal res)	.121°/µsec
Max Travel (out of box)	128°
Max Travel (reprogrammed normal res)	181°
Pulse Amplitude	3-5V
Operating Temperature	-20°C to +60°C
Current Drain - idle (4.8V)	3mA
Current Drain - idle (6.0V)	3mA
Current Drain - no-load (6V)	200mA
Current Drain - no-load (7.4V)	240mA
Current Drain - stall (4.8V)	2A
Current Drain - stall (6V)	3A
Continuous Rotation Modifiable	No
Direction w/ Increasing PWM Signal	Clockwise
Deadband Width	2µs
Motor Type	Carbon Brush
Potentiometer Drive	6 Slider Indirect Drive
Feedback Style	5KΩ Potentiometer
Output Shaft Support	Top Ball Bearing
Gear Type	Straight Cut Spur
Gear Material	Metal
Wire Length	7" (178mm)
Wire Gauge	28AWG

## C-11 Arduino UNO

# Technical Specification



EAGLE files: [arduino-duemilanove-uno-design.zip](#) Schematic: [arduino-uno-schematic.pdf](#)

## Summary

Microcontroller	ATmega328
Operating Voltage	5V
Input Voltage (recommended)	7-12V
Input Voltage (limits)	6-20V
Digital I/O Pins	14 (of which 6 provide PWM output)
Analog Input Pins	6
DC Current per I/O Pin	40 mA
DC Current for 3.3V Pin	50 mA
Flash Memory	32 KB of which 0.5 KB used by bootloader
SRAM	2 KB
EEPROM	1 KB
Clock Speed	16 MHz

## the board

